

Report #1

Submitted on 15 Sep 2015

Anonymous Referee #2

The new version of the paper was improved and I feel that authors provide relatively convincing answers to reviewer's comments. Useless figures were removed and a better description of the originality/novelty of the present paper compared to previous studies was done.

I regret that the paper doesn't show any quantitative comparison with Wanders et al. study, which would have been able to quantify the improvement of the method. In addition, I have still some difficulties to clearly understand some parts of the paper, and some figure legends really need a detailed description (see below). However, the paper shows some interesting findings related to soil saturation effect and precipitation threshold detectability on the quality of precipitation corrections. Thus, my recommendation is to publish the paper providing that the following minor/technical comments are addressed.

We would like to thank Anonymous Referee #2 for the comments. Please find our response below (comments by Referee #2 are quoted in blue italic and our response are marked in black. Line numbers are marked according to the updated manuscript with tracked changes).

We have included a quantitative comparison of FAR and POD with Wanders et al. and discussion of differences in methods used (line 565-603).

- The legend in Figure 2 should be detailed as it was done in Wanders et al. Only one line in the present paper (about 10 in Wanders) is not enough to correctly understand the Figure.*
 - Can authors better explain what the two circles in Figure 2 are?*
-

Figure 2 is updated with detailed description added in the caption and Line 183-184.

- Line 385: what is possibly due to lower soil moisture variability ...?! Reconsider the sentence.*
-

We revised the sentence in Line 369.

- The legend in Figure 12 should also be detailed to capture the main result of the figure.*
-

We included this information in the caption of Figure 12.

- Indicate the time-period in Figure 9 legend.*
-

The period is from 2003/01/01 to 2007/07/31. This has been clarified in the caption of figure 9.

Report #2

Submitted on 18 Sep 2015

Referee #1: Dr. Luca Brocca, luca.brocca@irpi.cnr.it

I found the paper significantly improved and the reviewers' comments successfully addressed. Specifically, the description of the method and of the results is now clear and detailed as needed (at least for me). The comparison with previous studies is also well done and highly interesting. The differences with Wanders et al. (2015) are now evident. Anyhow, I have completely re-read the paper and I still have some minor comments to be addressed.

We would like to thank Dr. Luca Brocca for the comments. Please find our response below (comments by Dr. Luca Brocca are quoted in blue italic and our response are marked in black. Line numbers are marked according to the updated manuscript with tracked changes).

1) *Lines 78-82: does it mean that it is better to use LST data with respect to soil moisture? It is not clear to me by reading this sentence.*

We revised the sentence in lines 80-82.

2) *At lines 83-93 it reads: "But this isn't always the case, and it is also noted that current low-frequency microwave soil moisture missions (specifically SMAP and SMOS) don't have radiometers at frequencies useful for estimating land surface temperatures, even though a 37 GHz sensor is part of the AMSR2 system. In fact SMAP and ECMWF/SMOS use LST from weather models analysis fields in their algorithms. Unfortunately the lowest microwave frequency of AMSR2 and SMOS precludes retrieving soil moisture from many areas with heavy vegetation, and AMSR2 has a significant dry bias with less availability than AMSR-E, but is no longer operable. So improvements to satellite precipitation from the Global Precipitation Mission products must rely solely on satellite soil moisture products from SMAP, which is promises better soil moisture retrievals due to increased penetration depth, and the improvements to the assimilation algorithms is the goal of this study."*
I found this paragraph unfair and also with some wrong sentences. I suggest strongly revise it. I do not believe it is a good justification the use of soil moisture, instead of LST, simply saying that current missions don't have frequencies useful for estimating land surface temperatures. It is not the case for AMSR2 (currently in orbit) and also for Chinese sensors. B) SMOS is operating at L-band as SMAP. Why SMOS should have a more problems than SMAP in highly vegetated areas? Why "ECMWF/SMOS" and not only SMOS? C) "So improvements to satellite precipitation from the Global Precipitation Mission products must rely solely on satellite soil moisture products from SMAP". This sentence is wrong and should be changed. D) Note also that scatterometer data from ASCAT are found to provide highly useful information for rainfall correction/retrieval in studies by Crow et al. and Brocca et al. I guess it should be acknowledged.

The reference in the original sentence regarding SMOS was inadvertently included, and we thank the reviewer for noting this. We have also edited the statement to better reflect our message. Thus our revised statement (now in line 83-94) now reads:

But this isn't always the case, and it is also noted that current low-frequency microwave soil moisture missions (specifically SMAP and SMOS) don't have radiometers at frequencies useful for estimating land surface temperatures, even though a 37 GHz sensor is part of the AMSR2 system. In fact SMAP and SMOS use LST from weather models analysis fields in their algorithms. Unfortunately the lowest microwave frequency of AMSR2 precludes retrieving soil moisture from many areas with heavy vegetation, and AMSR2 has a significant dry bias with less availability than AMSR-E, but is no longer operable. So improvements to satellite precipitation from the Global Precipitation Mission products must rely solely on satellite soil moisture products, and the improvements to the assimilation algorithms is the goal of this study

3) *Lines 219-220: is the correction made pixel by pixel? Please specify.*

The correction is done pixel by pixel. This has been clarified in line 226.

4) *Line 378: Please revise the sentence.*

We revised the sentence in line 380-381.

5) *Line 392: "Consistent with other studies" Add here the references to that studies.*

We added references in line 402.

- 6) *Lines 490-491: In Brocca et al. (2014) three global scale DAILY rainfall products are obtained from ASCAT, AMSR-E and SMOS soil moisture products. The performance is computed for 5-day cumulated rainfall as the temporal resolution of the sensors (mainly SMOS) was not suitable for high resolution (daily) rainfall estimation. Therefore, 5-day precipitation is not estimated by considering “soil moisture changed over a 5-day period”. Please change.*
-

We revised the text between lines 499 and 507 to clarify that the estimation algorithm results in the estimation of daily precipitation, and uses soil moisture observations from three satellite derived soil moisture datasets (AMSR-E LPRM, ASCAT and SMOS) whose values were linearly interpolated to daily values for the precipitation estimation algorithm.

Note also that recently in Ciabatta et al. (2015, JHM: <http://dx.doi.org/10.1175/JHM-D-14-0108.1>) daily rainfall product from ASCAT is obtained through the same approach in Brocca et al. (2014), and the integration of ASCAT-derived rainfall with TRMM provided significant improvements in all performance scores even for 1-day precipitation. Moreover, very recent results with accurate estimation of 1-day rainfall (still in preparation, not yet published on journals but only at conferences) are coming.

This has been acknowledged in line 508-510.

- 7) *Line 518-520: please revise the sentence, something seems missing.*
-

In re-reading these sentences, we agree with the reviewer that they are unclear. Since they don't add additional information, we have decided to remove them for readability.

1 **Correction of real-time satellite precipitation with**
2 **satellite soil moisture observations**

3

4 **Wang Zhan¹, Ming Pan¹, Niko Wanders^{1,2}, Eric F. Wood¹**

5 [1] Department of Civil and Environmental Engineering, Princeton University, Princeton,
6 NJ, USA

7 [2] Department of Physical Geography, Utrecht University, Utrecht, the Netherland

8

9 **Abstract**

10 Rainfall and soil moisture are two key elements in modeling the interactions between the
11 land surface and the atmosphere. Accurate and high-resolution real-time precipitation is
12 crucial for monitoring and predicting the on-set of floods, and allows for alert and
13 warning before the impact becomes a disaster. Assimilation of remote sensing data into a
14 flood-forecasting model has the potential to improve monitoring accuracy. Space-borne
15 microwave observations are especially interesting because of their sensitivity to surface
16 soil moisture and its change. In this study, we assimilate satellite soil moisture retrievals
17 using the Variable Infiltration Capacity (VIC) land surface model, and a dynamic
18 assimilation technique, a particle filter, to adjust the Tropical Rainfall Measuring Mission
19 Multi-satellite Precipitation Analysis (TMPA) real-time precipitation estimates. We
20 compare updated precipitation with real-time precipitation before and after adjustment
21 and with NLDAS gauge-radar observations. Results show that satellite soil moisture
22 retrievals provide additional information by correcting errors in rainfall bias. The
23 assimilation is most effective in the correction of medium rainfall under dry to normal
24 surface condition; while limited/negative improvement is seen over wet/saturated
25 surfaces. On the other hand, high frequency noises in satellite soil moisture impact the
26 assimilation by increasing rainfall frequency. The noise causes larger uncertainty in the

27 false-alarmed rainfall over wet regions. A threshold of 2 mm/day soil moisture change is
28 identified and applied to the assimilation, which masked out most of the noise.

29

30

31 **1 Introduction**

32 Precipitation is perhaps the most important variable in controlling energy and mass fluxes
33 that dominate climate and particularly the terrestrial hydrological and ecological systems.

34 Precipitation estimates, together with hydrologic models, provide the foundation for
35 understanding the global energy and water cycles (Sorooshian, 2004; Ebert et al., 2007).

36 However, obtaining accurate measurements of precipitation at regional to global scales
37 has always been challenging due to its small-scale, space-time variability, and the sparse
38 networks in many regions. Such limitations impede precise modeling of the hydrologic
39 responses to precipitation. There is a clear need for improved, spatially distributed
40 precipitation estimates to support hydrological modeling applications.

41 In recent years, remotely sensed satellite precipitation has become a critical data source
42 for a variety of hydrological applications, especially in poorly monitored regions such as
43 sub-Saharan Africa due to its large spatial coverage. To date, a number of fine-scale,
44 satellite-based precipitation estimates are now in operational production. One of the most
45 frequently used is the Tropical Rainfall Measuring Mission Multi-satellite Precipitation
46 Analysis (TMPA) product (Huffman et al., 2007). Over the 17 years lifetime since the
47 launch of the Tropical Rainfall Measuring Mission (TRMM) in 1997, a series of high
48 resolution (0.25-degree and 3-hourly), quasi-global (50°S - 50°N), near-realtime,
49 TRMM-based precipitation estimates have been developed and made available to the
50 research and applications communities (Huffman et al., 2007; 2010). Flood forecasting
51 and monitoring is one major application for real time satellite rainfall products (Wu et al,
52 2014). However, the applicability of satellite precipitation products for near real-time
53 hydrological applications that include drought and flood monitoring has been hampered
54 by their need for gauge-based adjustment.

55 While it is possible to create such estimates solely from one type of sensor, researchers
56 have increasingly moved to using combinations of sensors in an attempt to improve
57 accuracy, coverage and resolution. A promising avenue for rainfall correction is through
58 the assimilation of satellite-based surface soil moisture into a water balance model (Pan
59 and Wood, 2006). Over land, the physical relationship between variations in soil water
60 storage and rainfall accumulation contain complementary information that can be
61 exploited for the mutual benefit of both types of products (Massari et al., 2014; Crow et
62 al., 2009). Unlike instantaneous rain rate, satellite surface soil moisture retrievals utilize
63 low frequency microwave signals and possess some memory reflecting antecedent
64 rainfall amounts.

65 Studies have demonstrated that in situ (Brocca et al., 2009, 2013; Matgen et al., 2012)
66 and satellite (Francois et al., 2003; Pellarin et al., 2008, 2013; Brocca et al., 2014)
67 estimates of surface soil moisture could contribute to precipitation estimates by providing
68 useful information concerning the sign and magnitude of antecedent rainfall
69 accumulation errors. In particular, Brocca et al. (2014) estimated daily rainfall on a global
70 scale based on satellite SM products by inverting the soil water balance equation. Crow et
71 al. (2003, 2009, 2011) corrected space-borne rainfall retrievals by assimilating remotely
72 sensed surface soil moisture retrievals into an Antecedent Precipitation Index (API) based
73 soil water balance model using a Kalman filter (Kalman, 1960). However, these studies
74 focused on multi-day aggregation periods and a space aggregated correction at 1°
75 resolution for the corrected precipitation totals. This limits their applicability in
76 applications such as near real-time flood forecasting. Wanders et al. (2015) tried to
77 overcome this limitation by the correction of 3 hourly satellite precipitation totals with a
78 set of satellite soil moisture and land surface temperature observations. One important
79 conclusion by Wanders et al. (2015) is that their results showed the limited potential for
80 satellite soil moisture observations for correcting precipitation at high resolution if “all-
81 weather” – i.e. microwave based – land surface temperatures are not available
82 coincidentally, as was the case with AMSR-E.

83 But this isn't always the case, and it is also noted that current low-frequency microwave
84 soil moisture missions (specifically SMAP and SMOS) don't have radiometers at

Authors 10/2/2015 8:10 PM
Deleted: and at high spatial resolution

Authors 10/2/2015 8:10 PM
Deleted:

Authors 10/2/2015 8:10 PM
Formatted: hvr

Authors 10/2/2015 8:10 PM
Formatted: hvr

87 frequencies useful for estimating land surface temperatures, even though a 37 GHz sensor
88 is part of the AMSR2 system. In fact SMAP and SMOS use LST from weather models
89 analysis fields in their algorithms. Unfortunately the lowest microwave frequency of
90 AMSR2 precludes retrieving soil moisture from many areas with heavy vegetation, and
91 AMSR2 has a significant dry bias with less availability than AMSR-E, but is no longer
92 operable. So improvements to satellite precipitation from the Global Precipitation
93 Mission products must rely solely on satellite soil moisture products, and the
94 improvements to the assimilation algorithms is the goal of this study.

95 Thus, we focus exclusively on the usefulness of assimilating soil moisture products to
96 improve satellite rainfall. We propose as part of the work how to improve the generation
97 of rain particles and the bias-correction of the satellite soil moisture observations, as well
98 as to enhance the assimilation algorithm to maximize the information that can be gained
99 from using soil moisture alone to adjust precipitation. Due to the very strong and
100 complicated spatial structure of precipitation, that is non-Gaussian and non-stationary in
101 both time and space (Wanders et al., 2015), a more advanced method is applied to
102 generate possible precipitation fields than were used in earlier studies or in Wanders et al,
103 2015) (see section 2.2.2). Furthermore, a more advanced bias correction method is also
104 applied to account for the reported problems in the second order statistics of the soil
105 moisture retrievals. We used a soil moisture remote sensing product to improve real-time
106 remote sensing precipitation product, TMPA 3B42RT, through a Particle Filter (PF) and
107 therefore offer an improved basis for quantitatively monitoring and predicting flood
108 events, especially in those parts of the world where in-situ networks are too sparse to
109 support more traditional methods of hydrologic monitoring and prediction. The
110 precipitation enhancement experiments are carried out over the continental U.S.
111 (CONUS) and the precipitation skill is validated against the NLDAS gauge-radar
112 precipitation product. Section 5 presents a comparison of the results from this study to
113 the earlier studies related to improving satellite precipitation.

Authors 10/2/2015 8:10 PM

Deleted: ECMWF/

Authors 10/2/2015 8:10 PM

Deleted: and SMOS

Authors 10/2/2015 8:10 PM

Deleted: from SMAP, which is promises better soil moisture retrievals due to increased penetration depth

119 **2 Methods**

120 **2.1 Overview**

121 Random replicates of satellite precipitation are generated based on real-time TMPA
122 (3B42RT) retrievals and its uncertainty (Pan et al., 2010), which are then used to force
123 the VIC land surface model (LSM) where one output of interest is surface soil moisture.
124 Satellite soil moisture data products are compared and merged with the 3B42RT product
125 to improve the accuracy of the satellite precipitation estimates. A schematic for the study
126 approach is provided in Figure 1. Based on real-time 3B42RT retrievals, a set of possible
127 precipitation estimates (a.k.a. replicates or particles) $\{p^i\}_{i=1,2,\dots,N}$ is generated with
128 assigned initial prior probability weights $\{w^i\}_{i=1,2,\dots,N}$. These rainfall rates are then used
129 to force the VIC land surface model to produce soil moisture predictions $\{\theta^i\}_{i=1,2,\dots,N}$.
130 Retrievals of AMSR-E satellite surface soil moisture using the Land Surface Microwave
131 Model (LSMEM) (Pan et al., 2014) are then merged with the LSM-based soil moisture
132 within the Particle Filter (PF) that compares AMSR-E/LSMEM changes in soil moisture,
133 ΔSM , to the LSM predicted soil moisture changes. From these, posterior weights
134 $\{w^{i+}\}_{i=1,2,\dots,N}$ are calculated for each precipitation member (particle) that takes into
135 account the uncertainties of AMSR-E/LSMEM ΔSM retrievals. From these updated
136 weights, an updated precipitation probability distribution is constructed, where the
137 precipitation particle with highest probability is taken as the “best” adjusted precipitation
138 estimate ($3B42RT_{ADJ}$). The procedure is carried out over the continental US (CONUS)
139 region on a grid-by-grid basis (0.25-degree) and a daily time step. Allowing for 6 months
140 model spin-up period, the adjustment is done from January 2003 to July 2007.

141 **2.2 Modeling, Statistical Tools and Data Sources**

142 **2.2.1 The Particle Filter**

143 Data assimilation methods are capable of dynamically merging predictions from a state
144 equation (i.e. the land surface model) with measurements (i.e. AMSR-E retrievals) to
145 minimize uncertainties from both the predictions and measurements. It is assumed that

146 the source of uncertainty in the land surface model predictions come solely from the real-
 147 time satellite precipitation, so that the particle filter (PF) provides an algorithm to update
 148 the precipitation based on the AMSR-E retrievals. The state evolution of a particle filter
 149 from discrete time $t-1$ to t can be represented as:

$$150 \quad \theta_t = f_t(\theta_{t-1}, p_t, \kappa_t, \alpha_t) \quad (1)$$

151 where θ_t is the 1st layer soil moisture at time t , whose value is predicted by the state
 152 equation Eq.(1) as $f_t(\bullet)$, and in the study is the hydrological model VIC, which takes in
 153 forcing data, including precipitation (p_t) and other forcings (κ_t); and simulates land
 154 surface states (soil moisture and soil temperatures at various levels, snow, etc.) and fluxes
 155 (evapotranspiration, runoff) at time t . Herein we are basically interested only in the 1st
 156 layer (top 10cm) soil moisture state and precipitation forcing, so other states and fluxes
 157 are not explicitly shown. α_t is the random error in the prediction of θ_t , whose statistics
 158 are known but not its value at any specific time.

159 At time t , the satellite surface soil moisture retrieval, θ_t^* , can be related to the VIC
 160 modeled 1st layer soil moisture θ_t as:

$$161 \quad \theta_t^* = h_t(\theta_t, \beta_t) \quad (2)$$

162 where h_t is taken as a regression that transforms the VIC simulated 1st layer soil
 163 moisture to satellite surface soil moisture. β_t is the noise in this regression relationship.
 164 The two noises α_t and β_t are assumed to be independent of each other at all times t .

165 At time t , given a 3B42RT precipitation estimate, p_t^{sat} , a set of N precipitation replicates
 166 $\{p_t^i\}_{i=1,2,\dots,N}$ and their associated initial prior probability weight $\{w_t^i\}_{i=1,2,\dots,N}$ are
 167 generated.

$$168 \quad g(p_t^{\text{sat}}) \sim \{p_t^i, w_t^i\}_{i=1,2,\dots,N} \quad (3)$$

$$169 \quad \sum_{i=1}^N w_t^i = 1 \quad (4)$$

170 $g(\cdot)$ is a probability density function. For N precipitation replicates, $\{p_t^i\}_{i=1,2,\dots,N}$, the
 171 propagation of the states from time step $(t-1)$ to t is by the VIC land surface model

172 represented in Eq.(1). The VIC land surface model simulates the 10cm 1st layer soil
173 moisture, $\{\theta_t^i\}_{i=1,2,\dots,N}$ for each precipitation replicate.

$$174 \quad \{\theta_t^i = f_t(\theta_{t-1}, p_t^i, \kappa_t, \alpha_t)\}_{i=1,2,\dots,N} \quad (5)$$

175 with the associated weights assigned to the precipitation member:

$$176 \quad \{\theta_t^i, w_t^i\}_{i=1,2,\dots,N} = \{f_t(\theta_{t-1}, p_t^i, \kappa_t, \alpha_t), w_t^i\}_{i=1,2,\dots,N} \quad (6)$$

177 If the satellite soil moisture retrieval at time t is θ_t^* , the update of precipitation forcing is
178 accomplished by updating the importance weight of each replicate given the
179 “measurement” θ_t^* :

$$180 \quad w_t^{i+} \sim \{g(\theta_t^i | \theta_t^*)\}_{i=1,2,\dots,N} \quad (7)$$

$$181 \quad \sum_{i=1}^N w_t^{i+} = 1 \quad (8)$$

182 The likelihood function $g(\theta_t^i | \theta_t^*)$ can be derived from h_t and $g(\beta_t)$. The schematic of the
183 utilized strategy is shown in Figure 2, [with a synthetic example of a missing rainfall](#)
184 [pattern in the TMPA compared with satellite \$\Delta\$ SM](#). The primary disadvantage of the
185 particle filter is the large number of replicates required to accurately represent the
186 conditional probability densities of p_t and θ_t . When the measurements exceed a few
187 hundred, the particle filter is not computationally practical for land surface problems.
188 Considering computation efficiency, we set the number of independent particles, N, from
189 the prior distribution to be 200.

190 **2.2.2 Precipitation Replicates Generation**

191 We generate precipitation replicates, $\{p_t^i\}_{i=1,2,\dots,N}$, based on statistics comparing NLDAS
192 and 3B42RT precipitation, as shown in Figure 3. Given a 3B42RT precipitation
193 measurement (binned by magnitude), with bin minimum and maximum indicated in
194 Figure 3, precipitation replicates are generated based on the corresponding 15th, 30th, 70th,
195 85th percentiles and the maximum NLDAS precipitation of the particular quantile bin as
196 follows: 15% of the replicates are generated with values uniformly distributed from 0 and
197 15th percentile; 15% of replicates with values from 15th to 30th percentile; 20% of
198 replicates with values from 30th percentile to the median; 20% of the replicates generated

Authors 10/2/2015 8:10 PM

Deleted: .

200 from the median to 70th ; 15% with values from 70th to 85th percentile; and 15% from the
201 85th percentile to the maximum precipitation value. Note that although the generation of
202 particles is based on statistics calculated from NLDAS, results show little difference
203 generating precipitation ensembles uniformly distributed between 0 and 200 mm/day.

204 **2.2.3 AMSR-E/LSMEM Soil Moisture Retrievals**

205 The soil moisture product is derived from multiple microwave channels of the Advanced
206 Microwave Scanning Radiometer for EOS (AMSR-E) instrument. The retrieval algorithm
207 by Pan et al. (2014) is an enhanced version of the Land Surface Microwave Emission
208 Model (LSMEM). The near surface soil moisture and vegetation optical depth (VOD) are
209 estimated simultaneously from a dual polarization approach that utilizes both horizontal
210 (H) and vertical (V) polarizations measurement by the space-borne sensor. The input
211 AMSR-E brightness temperature comes from the NSIDC AMSR-E/Aqua Daily Global
212 Quarter-Degree Gridded Brightness Temperatures product (overlapping swaths in the
213 same day are truncated so that only the latest one is present). Consequently, the soil
214 moisture retrievals are also gridded at 0.25-degree with one ascending map and one
215 descending map at the daily time step. A maximum threshold value of 0.6 m³/m³ has been
216 applied manually to reduce error from open water bodies. According to Pan et al. (2014),
217 the soil moisture dataset based on observations from AMSR-E are shown to be consistent
218 at large scales in terms of reproducing the spatial pattern of soil moisture from VIC land
219 surface model simulation. Ascending soil moisture retrievals (equatorial crossing time
220 1:30PM local time) is assimilated in this study.

221 Similarly, while the spatial patterns of the basic statistics of AMSR-E/LSMEM SM
222 retrievals compare well to VIC simulations (Pan et al., 2014), VIC has its top layer (10
223 cm), which is deeper than the detection depth of AMSR-E, so that the mean and temporal
224 variability of the retrievals are higher than the VIC simulated soil moisture (Figure 4 in
225 Pan et al., 2014). Considering this difference between detection depths, we pre-process
226 soil moisture retrievals [for each pixel](#) as follows:

227 1) Rescale soil moisture retrievals (AMSR-E/LSMEM SM) to have the same minimum
228 and maximum range as VIC simulated 1st layer soil moisture.

229 2) Calculate a daily soil moisture change. As satellite retrievals are manually truncated to
230 be no more than $0.6 \text{ m}^3/\text{m}^3$ (equivalent to 60mm of water in the top soil layer in VIC),
231 retrievals larger than $0.6 \text{ m}^3/\text{m}^3$ are excluded.

232 3) Fit a 2nd order polynomial regression model with ΔSM (all units in mm of water in the
233 top layer) from satellite and VIC simulation on a monthly basis and 3×3 grid scale
234 (window).

235 After pre-processing, the distribution of soil moisture change matches fairly well with
236 $\Delta\text{SM}_{\text{VIC}}$ (Figure 4). The mean absolute difference reduces from a spatial average of 5.25
237 mm/day to 0.71 mm/day, with relatively larger value over eastern CONUS. According to
238 Pan et al. (2014), the no-skill or negative-skill areas occur mostly over eastern dense
239 forests due to vegetation blockage of the soil moisture signal (Pan et al., 2014). The
240 accuracy of soil moisture retrievals is also limited by mountainous topography and the
241 occurrence of snow and frozen ground during winter whose identification from satellite
242 observations is often difficult. For the purpose of this study, we assign zero weight to the
243 $3\text{B42RT}_{\text{ADJ}}$ and rely exclusively on the initial 3B42RT precipitation for time steps when
244 the VIC model predicts snow cover or frozen surfaces.

245 **2.2.4 VIC Land Surface Model**

246 The Variable Infiltration Capacity (VIC) model (Liang et al., 1994; Gao et al., 2010) is
247 used to dynamically simulate the hydrological responses of soil moisture to precipitation,
248 surface radiation and surface meteorology. The VIC model solves the full energy and
249 water balance over each 0.25-degree-grid-cell independently, thus ensuring its
250 computational efficiency. The assumption of independency poses limitation on the
251 application of LSM at very high spatial resolution (e.g. $1\text{km}\times 1\text{km}$) over large areas.
252 Three-layer-soil-moisture is simulated through a soil-vegetation-atmosphere transfer
253 (SVAT) scheme, which also accounts for sub-grid scale heterogeneity of vegetation, soil
254 and topography. A detailed soil moisture algorithm description can be found in Liang et
255 al. (1996). The VIC model has been validated extensively over CONUS by evaluating
256 soil moisture and simulations to observations (Robock et al., 2003; Schaake et al., 2004).

257 **3 Idealized Experiment**

258 Before applying the Particle Filter assimilation algorithm on 3B42RT precipitation
259 estimates, we conducted an idealized experiment where we treat the NLDAS
260 precipitation as the “truth” and the NLDAS precipitation forced VIC simulations as
261 “satellite observed” soil moisture. As an idealized experiment, we adjust TMPA real-time
262 precipitation estimates based on these “satellite observations”. Phase 2 of the North
263 American Land Data Assimilation System (NLDAS-2) rainfall forcing combines hourly
264 WSR-88D radar analyses from the National Weather Service (NWS) and daily gauge
265 reports (~13,000/day) from the Climate Prediction Center (CPC) (Ek et al., 2011). The
266 dataset, with a spatial resolution of 0.125 degree and hourly observations, was pre-
267 processed into 0.25-degree daily precipitation to be consistent with that of 3B42RT and
268 AMSR-E/LSMEM SM datasets. Hourly NLDAS and 3-hourly 3B42RT precipitation is
269 aggregated into daily precipitation defined by a period shifted ~7.5 hours into the future
270 (9:00PM-9:00PM), allowing for a necessary delay for soil moisture to respond to
271 incoming rainfall. The idealized experiment is designed to test whether the algorithm is
272 able to retrieve rainfall forcing with soil moisture change, assuming that the soil moisture
273 observations are 100% accurate.

274 Results show that, with the knowledge of 1st layer soil moisture change (via the “satellite
275 observations”), the adjustment is able to recover intensity and spatial pattern of forcing
276 precipitation (Figure 5g). Average mean absolute error (MAE) of daily rainfall amount is
277 reduced by 52.9% (2.91 mm/day to 1.37 mm/day) over the region. Figure 5a to Figure 5e
278 shows an example of the recovered rainfall field from the idealized experiment for 27th
279 Oct. 2003. The spatial pattern matches the original NLDAS precipitation well.

280 **3.1 Effect of surface soil saturation**

281 While successfully recovering the general pattern of NLDAS precipitation based on first
282 layer soil moisture, the idealized experiment is not always able to recover the
283 precipitation volume due to the fact that the top layer soil moisture alone does not contain
284 the complete memory of the previous day’s rainfall. Deeper soil moisture,
285 evapotranspiration and runoff also carry part of this information. As the surface gets

286 wetter, the VIC 1st layer soil moisture has smaller variation. If the incoming precipitation
287 brings the surface to saturation, the VIC model redistributes the soil moisture vertically
288 through vertical moisture flow and generates runoff. Hence soil moisture increments,
289 ΔSM , near saturation are less correlated with incoming precipitation as they change
290 minimally to additional incoming rainfall. An example demonstrating this saturation
291 effect is shown in Figure 5f to Figure 5j. When incoming precipitation brings the surface
292 SM to (near) saturation, there is very limited improvement after the adjustment. Because
293 of the low sensitivity of the soil surface to precipitation, there is little change in ΔSM in
294 response to precipitation variations among the replicates. It is almost always the case that
295 the algorithm is not able to find a “matching” ΔSM .

296 We separately evaluate the skill improvement in the recovered NLDAS precipitation with
297 and without surface saturation. Figure 6 confirms the effect of surface saturation on
298 adjusted precipitation, which is well described in previous studies (e.g. Brocca et al.,
299 2013, 2014). The recovered precipitation, when the surface soil is saturated, only
300 contributes more noise rather than an improvement to the rainfall estimates. The VIC
301 model computes the moisture flow between soil layers using an hourly time step. If the 1st
302 layer soil moisture exceeds its maximum capacity, it is considered to be a surface
303 saturation case. As seen in Figure 5, there is very limited or negative skill in the
304 recovered precipitation under saturated surface soil moisture conditions. Such
305 circumstances are identified and the AMSR-E/LSMEM ΔSM observation disregarded by
306 assigning zero weight to the $3B42RT_{ADJ}$ values. Thus for wetter areas with heavy
307 precipitation that potentially would bring the surface soil moisture to saturation, the
308 $3B42RT$ product is less likely to be adjusted according to satellite ΔSM and the best
309 precipitation estimate is $3B42RT$.

310 **3.2 Effect of SM uncertainty**

311 In the idealized experiment, NLDAS-VIC soil moisture is taken as truth with zero
312 uncertainty associated with (θ_t^*) . However, this assumption is not valid for real satellite
313 SM retrievals, mean absolute error of which is approximately 3% vol./vol. (McCabe et
314 al., 2005). To consider this, we added error to the “truth” SM (normally distributed with
315 zero mean and standard deviations of 1mm, 2mm, 3mm, 4mm and 5mm), and simulated

316 the effect of SM uncertainty to evaluate the associated adjustment errors. Figure 7 shows
317 that larger soil moisture observation errors lead to larger error variation after adjustment.
318 This also suggests that soil moisture responds to precipitation non-linearly based on
319 different initial conditions. An estimated wetter surface has lower sensitivity to an
320 incoming rainfall amount, resulting in larger error in the recovered NLDAS precipitation.
321 As shown in Figure 7, the error standard deviation of the recovered NLDAS precipitation
322 increases with surface water content (statistics shown in Table 2). As we add noise larger
323 than $N(0,1\text{mm})$ into “true” SM observation, there is a wet bias of approximately 1
324 mm/day regardless of 1st layer soil moisture level. This suggests that when the difference
325 between 1st layer SM and saturation is less than 8 mm, the median of the errors in the
326 recovered NLDAS precipitation grows from 0.16 mm/day to 1.89 mm/day when we add
327 $N(0,5\text{mm})$ noise, while inter-quantile range (IQR) increases from 1.71 mm/day to 7.04
328 mm/day. Acknowledging such a wet bias, to avoid introducing any more unintentional
329 bias in the $3B42RT_{\text{ADJ}}$ estimates, we take as zero the uncertainty of AMSR-E/LSMEM
330 SM retrievals, i.e. we take $h_t(\theta_t)$ as our single observation θ_t^* and adjust the $3B42RT$
331 estimates accordingly.

332 It is noteworthy that the soil moisture change is calculated based on previous days’ soil
333 water contents. Therefore errors tend to accumulate over time until they are “re-set” when
334 a significant precipitation event takes place. This type of uncertainty accounts for a small
335 portion of the total error in the adjusted precipitation (black being the no error case in
336 Figure 7 with the “true” change in soil moisture from every time step). As complete
337 global coverage is not provided with each orbit of the AMSR-E sensor, on average 44.01%
338 of the time steps ($<0.6 \text{ m}^3/\text{m}^3$) during the study period have observations, with more
339 frequent overpasses at higher latitudes (Figure 4e in Pan et al., 2014). This observation
340 gap unavoidably introduces extra uncertainty in the retrieval of the precipitation signal.
341 To further avoid possible additional errors, we update the forcing rainfall when a ΔSM
342 temporal match ($\pm 0.4\text{mm}$) is available, and keep the original precipitation if a match isn’t
343 available.

344 **4 Improvement on real-time precipitation estimates and their validation**

345 The adjustment of real TMPA 3B42RT retrievals based on AMSR-E/LSMEM Δ SM is
346 carried out using the methods described in Section 2.2.3, and results from the idealized
347 experiment (Sect. 3) with regard to the circumstances where an adjustment is applied.

348 An example of TMPA 3B42RT adjustment is provide in Figure 8, where a snapshot of
349 the rainfall field is shown (Figure 8b) and compared with NLDAS on May 26th 2006 and
350 the adjusted rainfall pattern based on AMSR-E/LSMEM Δ SM. The 3B42RT_{ADJ} rainfall
351 field (Figure 8c) is similar in terms of its spatial distribution compared to NLDAS
352 precipitation estimates (Figure 8d).

353 On average TMPA 3B42RT and AMSR-E/LSMEM Δ SM have a spatial Pearson
354 Correlation Coefficient of 0.37 (Shown in Figure 9, left), compared to 0.52 for the
355 correlation between NLDAS and Δ SM. After the adjustment procedure, the Pearson
356 correlation coefficient between 3B42RT_{ADJ} and AMSR-E/LSMEM Δ SM increases to
357 0.53 (shown in Figure 9), indicating that the correction method is successful. A below
358 average increase in correlation is found over the western mountainous region, the Great
359 Lakes region and eastern high vegetated and populated region. Additionally, the satellite
360 soil moisture suffers from snow/ice/standing water contamination, which affects the
361 potential for improved results after correction. The 3B42RT_{ADJ} has significant
362 improvement over 3B42RT in terms of long-term precipitation bias. The bias in 3B42RT
363 annual mean precipitation is reduced by 20.6%, from -9.32mm/month spatial average in
364 3B42RT to -7.40mm/month in 3B42RT_{ADJ} (shown in Figure 9, right). Frequency of rain
365 days generally increases significantly everywhere (Figure 10). The NLDAS data (Figure
366 10, right) suggests an almost constant drizzling rainfall over parts of the western
367 mountainous area (Montana, Idaho, Wyoming and Colorado), while assimilating AMSR-
368 E/LSMEM Δ SM datasets does not have a signal of higher rainfall frequency (Figure 10,
369 middle). This is possibly due to deficiencies in satellite retrievals over the mountainous
370 areas and frequent presence of snow and ice (3B42RT is not updated under such
371 circumstances).

372 Figure 11 shows the assimilation results for the grids and days with soil moisture
373 observations, using the NLDAS precipitation as a reference. Overall, the method is

Authors 10/2/2015 8:10 PM

Deleted: lower soil moisture variability

Authors 10/2/2015 8:10 PM

Deleted: dry,

376 successful in correcting daily rainfall amount when 3B42RT overestimates precipitation
377 (3B42RT - NLDAS > 0). Mean standard deviation (STD) of 3B42RT_{ADJ}-NLDAS is
378 between 1 and 3 mm/day (statistics provided in Table 3). When 3B42RT underestimates
379 rainfall (3B42RT - NLDAS < 0), the assimilation has limited improvement on 3B42RT.

380 This is due to the effect of surface saturation. In terms of adding rainfall, effectiveness of
381 the assimilation is limited under the following two circumstances.

382 1) The presence of wet conditions or (near) saturation. There is higher probability
383 bringing the surface to saturation (wetter condition) when the assimilation adds
384 rainfall into 3B42RT. However soil moisture increments are less sensitive to
385 incoming precipitation on wetter soil. Therefore, an error in ΔSM often translates into
386 3B42RT_{ADJ} in a magnified manner.

387 2) The presence of very heavy precipitation, which typically brings the surface to
388 saturation, hence not results in an update of 3B42RT, is not updated. If, by a small
389 probability, the surface is wet (nearly saturated) but not completely saturated after a
390 heavy rainfall, the updated 3B42RT also suffers from large uncertainty (explained in
391 1) above).

392 The effect of the assimilation conditioned on 3B42RT rainfall amount is further evaluated
393 by skill scores. Figure 12 presents probability of detection (POD) and false alarm rate
394 (FAR) in 3B42RT and 3B42RT_{ADJ}, using NLDAS as the reference dataset. The rain event
395 threshold is set to be 0.1 mm/day and 2 mm/day. This is possibly due to lower soil
396 moisture variability in satellite retrievals over the dry, mountainous areas and frequent
397 presence of snow and ice (3B42RT is not updated under such circumstances). For a 0.1
398 mm/day threshold, both FAR and POD increases in 3B42RT_{ADJ} except for the
399 mountainous region. Whereas for a 2 mm/day threshold, there is only slight increase in
400 FAR in most of eastern U.S. region. The overestimation of rain days is also absent when
401 2 mm/day event threshold is applied which suggests that most of the excessive rainy days
402 have less than 2 mm/day rain amount. Consistent with Wanders et al. (2015), spatially,
403 larger improvements are found in the central U.S. The area coincides where higher
404 AMSR-E/LSMEM ΔSM accuracy is found (non-mountainous regions with little
405 urbanization and light vegetation). Despite of the regional variability, these excessive

Authors 10/2/2015 8:10 PM

Deleted: there are two scenarios when the

Authors 10/2/2015 8:10 PM

Deleted: other studies,

408 rainy days are a result of the high-frequency noise in AMSR-E/LSMEM soil moisture
409 retrievals identified by Pan et al (2004) and Wanders et al. (2015).

410 The applied method is ineffective for light rainfall < 2 mm, where the adjustment tends to
411 over-correct precipitation by adding excessive rainfall – mostly the result of the high
412 frequency AMSR-E noise. MAE of light rainfall (< 2 mm/day) increased from 0.65
413 mm/day in 3B42RT to 0.99 mm/day in 3B42RT_{ADJ}. On the other hand, satellite soil
414 moisture assimilation is very effective in correcting satellite precipitation larger than 2
415 mm/day: MAE of medium to large rainfall (≥ 2 mm/day) decreased from 7.07 mm/day in
416 3B42RT to 6.55 mm/day in 3B42RT_{ADJ}. The effect of the assimilation is different over
417 the western mountainous region, the north-to-south central U.S. band and the eastern U.S.

418 The western mountainous region has a dry climatology with more frequent rainfall in
419 small amounts. The white noise in Δ SM, negatively impacting 3B42RT_{ADJ}, is comparable
420 to the positive improvement brought by actual light rainfall signals in Δ SM. Therefore,
421 the assimilation of Δ SM has no significant impact in these regions.

422 The north-to-south band over central U.S. experiences more medium to large (≥ 2
423 mm/day) rainfall. In addition, the region is lightly vegetated (annual mean LAI < 1) with
424 low elevation (< 1500 m), where soil moisture retrievals are of higher accuracy. Soil
425 moisture climatology is wetter in the west, causing larger variations in 3B42RT_{ADJ} error
426 from the white noise Δ SM (as discussed in Section 3.2). Despite of that, satellite soil
427 moisture is most effective correcting medium to large rainfall under normal surface
428 conditions.

429 The decreased skill in 3B42RT_{ADJ} over eastern U.S. is primarily attributed to both
430 precipitation and soil moisture climatology, a wet climate with more medium to large
431 rainfall, neither of which is suitable for soil moisture assimilation.

432 In summary, the high-frequency noise in soil moisture product causes a major limitation.
433 The noise impacts adjusted precipitation by introducing false alarm rain days. It is
434 difficult to distinguish the noise and retrieve the true rainfall signals. A remedy to prevent
435 the excessive rain days is applying a cutoff Δ SM threshold when rain days are added, at
436 the expense of neglecting a part of the true rainfall signals. Figure 13 shows the
437 probability of added rainy days being consistent with NLDAS (NLDAS > 0 mm/day)

438 with respect to ΔSM . When a new rainy day is added ($3B42RT = 0$ mm/day, $3B42RT_{ADJ}$
439 > 0 mm/day) based on AMSR-E/LSMEM ΔSM of 2 mm/day, there's approximately 78%
440 chance that the added rain day is a true event (NLDAS > 0 mm/day); That is, approx.
441 22% chance that it is a false alarm (NLDAS = 0 mm/day). When AMSR-E/LSMEM
442 ΔSM is larger than 2 mm/day, the probability of added rainy days being true event is
443 even higher, up to 90% chance. Here we applied a threshold of 2 mm/day on AMSR-
444 E/LSMEM ΔSM . That is, when new rainy days are introduced ($3B42RT > 0$,
445 $3B42RT_{ADJ} > 0$), we discard the update and keep the no-rain day if AMSR-E/LSMEM
446 soil moisture increment is below 2 mm. Note that, the probability of the false alarms
447 depends on soil moisture climatology: the wetter soil moisture climatology, the larger
448 uncertainty in the signal. Therefore, this threshold should vary in accordance with local
449 soil moisture climatology, i.e. a larger threshold over the wetter east U.S. and smaller
450 threshold over the drier western U.S. Nevertheless, after the 2 mm/day ΔSM threshold is
451 applied, expectedly, the statistics are largely improved: FAR is decreased significantly
452 from 0.519 (wo. ΔSM threshold) to 0.066 (w. ΔSM threshold). MAE of light rainfall (< 2
453 mm/day) in $3B42RT_{ADJ}$ decreased from 0.99 mm/day to 0.64 mm/day, compared to 0.65
454 mm/day in $3B42RT$. For medium to large $3B42RT$ rainfall (≥ 2 mm/day), it effectively
455 increased POD (0.362 in $3B42RT$ vs 0.386 in $3B42RT_{ADJ}$ w. ΔSM threshold) and
456 decreased FAR (0.037 in $3B42RT$ vs 0.030 in $3B42RT_{ADJ}$ w. ΔSM threshold). Further
457 work is needed to characterize, distinguish and decrease the high-frequency noise in SM
458 retrievals. Figure 13 gives an example of evaluating the impact of SM uncertainties in
459 assimilation as curves derived over different topography can be quantitatively compared.

460 **5 Comparison to other studies**

461 Many other studies have utilized satellite microwave brightness temperatures or soil
462 moisture retrievals to constrain satellite precipitation estimates (Pellarin et al., 2008),
463 estimate precipitation (e.g. Brocca et al., 2013) or improve precipitation estimates
464 through assimilation (Crow et al., 2009, 2011). Here, we review their approaches and
465 findings in light of the results of this study, and compare our results with some of these
466 studies to gain insight into their robustness and consistency.

467 Pellarin et al. (2008) used the temporal variations of the AMSR-E 6.7 GHz brightness
468 temperature (TB) normalized polarization difference, $PR=(TB_V-TB_H)/(TB_V+TB_H)$, to
469 screen out anomalous precipitation events from a 4-day cumulative satellite-estimated
470 precipitation (EPSAT-SG: Chopin et al., 2005) from 22 to 26 of June 2004 over a 100 x
471 125 km box centered over Niger in west Africa. This was extended in Pellarin et al.
472 (2013) where an API-based water balance model was used to correct three different
473 satellite precipitation products (CMORPH, TRMM-3B42 and PERSIANN) over a 4-year
474 period in west Africa at three 0.25° grids in Niger, Benin and Mali). The new algorithm
475 was evaluated by comparing the corrected precipitation to estimates over the 0.25° grids
476 from ground-based precipitation measurements. A sequential assimilation approach was
477 applied where AMSR-E C-band TB measurements were used to estimate a simple
478 multiplicative factor to the precipitation estimates in order to minimize the difference
479 between observed (AMSR-E) and simulated TBs in term of root mean square error
480 (RMSE). The results show improvements over those found in Pellarin et al. (2009).
481 Specifically, the Pellarin et al. (2013) study shows that the proposed methodology
482 produces an improvement of the RMSE at daily, decadal and monthly time scales and at
483 the three locations. For instance, the RMS mean error decreases from 7.7 to 3.5 mm/day
484 at the daily time scale in Niger and from 18.3 to 7.7 mm/day at the decadal time scale in
485 Mali.

486 Crow et al. (2003, 2009, 2011) demonstrated the effectiveness of the assimilation of
487 remotely sensed microwave brightness temperatures or retrieved soil moisture in
488 estimating precipitation based on airborne measurements over the Southern Great Plains
489 (USA) region (Crow et al., 2003); 2 to 10 day accumulated precipitation within a simple
490 API water budget model and assimilation scheme over CONUS (Crow et al., 2009); and
491 3 day, 1° precipitation accumulation over three African Monsoon Multidisciplinary
492 Analysis (AMMA) sites in west Africa with an enhanced assimilation scheme and an
493 API-moisture model (Crow et al., 2011). Crow et al. (2009) recommends against
494 estimating precipitation at a larger scale than three days based on assimilating AMSR-
495 E/LSMEM soil moisture.

496 Brocca et al. (2013) estimated precipitation by inverting the water budget equation such
497 that precipitation could be estimated from changes in soil moisture. The inverted equation

498 was calibrated using in-situ, 4-day averaged observations at two sites in Spain and Italy.
499 In Brocca et al. (2014), the same approach was used globally to estimate daily
500 precipitation at 1° spatially. 5 Day cumulated rainfall estimates are derived from three
501 satellite derived soil moisture datasets (AMSR-E LPRM, ASCAT and SMOS), and
502 linearly interpolated to daily values, for their precipitation estimation algorithm. No
503 formal data assimilation was carried out. The newly created precipitation data set was
504 compared to two satellite precipitation products (TRMM-3B42RT, GPCC) and two gauge
505 based precipitation products (GPCP, ERA-Interim). Five-day accumulated rainfall data,
506 aggregated to a 1° spatial resolution, are considered in their assessment analyses with
507 promising results. But they do note that their approach has “poor scores in reproducing
508 daily rainfall data”. Ciabatta et al. (2015) derived daily rainfall product using ASCAT
509 over Italy and integrated with TMPA 3B42RT precipitation. The merged product also
510 shows promising results.

511 In the study reported here, four advances have been made over these earlier studies: (i)
512 we adopted a state-of-the-art dynamic land surface model that has demonstrated high skill
513 in simulating soil moisture when driven by high quality precipitation data (Schaake et al.,
514 2004); (ii) we applied a state-of-the-art data assimilation procedure based on particle
515 filtering so as to extract (and hopefully maximize) the information content from the
516 satellite most effectively; (iii) we increased the resolution of the precipitation estimation
517 window down to 1 day, exceeding the conclusions in these earlier studies that the finest
518 temporal resolution is 3 to 5 days. Additionally we increased (or matched) the spatial
519 resolution to 0.25°, limited primarily by the satellite soil moisture product resolution; and
520 (iv) previous studies are based on the assumption that the SM retrievals are 100%
521 accurate and contain no errors. We evaluated this assumption by analyzing the impact of
522 uncertainties associated with the soil moisture retrievals. These advances offer important
523 benefits when satellite precipitation products are used for applications such as flood
524 forecasting. Admittedly by aggregating in space and time, the improvement is more
525 robust since some errors are averaged out.

526 Wanders et al. (2015) performed a comprehensive inter-comparison study using multiple
527 satellite soil moisture and land surface temperature (LST) data at fine temporal scale (3-
528 hourly). Compared to their study, ours focuses on using soil moisture exclusively from

Authors 10/2/2015 8:10 PM

Deleted: for 5-day

Authors 10/2/2015 8:10 PM

Deleted: totals and

Authors 10/2/2015 8:10 PM

Deleted: Soil moisture observations

Authors 10/2/2015 8:10 PM

Deleted:) were used. The soil moisture and rainfall were aggregated to a 1° spatial resolution, the soil moisture changes over a 5-day period

Authors 10/2/2015 8:10 PM

Deleted: estimate a 5-day total

Authors 10/2/2015 8:10 PM

Deleted: Nonetheless, these studies show

Authors 10/2/2015 8:10 PM

Deleted: three

Authors 10/2/2015 8:10 PM

Deleted: However improving satellite precipitation by AMSR-E/LSMEM SM is not entirely without skill. In fact, it could effectively correct rainfall with proper cautions given to local climatology where the assimilation is carried out.

545 one satellite and retrieval algorithm, and in improvements to the assimilation algorithm.
546 Specifically, (i) the longer temporal period (2010-2011 in Wanders, et al. versus 2002-
547 2007 in this study), (ii) the temporal resolution (3-hourly versus daily); (iii) the particle
548 generation and bias correction method. We present in the paper improvements in the
549 generation of rain particles and the bias-correction of the satellite soil moisture
550 observations, as well as enhancements to the assimilation algorithm to maximize the
551 information that can be gained from using soil moisture alone in adjusting precipitation.
552 Due to the very strong and complicated spatial structure of precipitation, that is non-
553 Gaussian and non-stationary in both time and space, a more advanced method is applied
554 to generate possible precipitation fields than used or presented in earlier studies or in
555 Wanders et al, (2015). Furthermore, a more advanced bias correction method is also
556 applied to account for the reported problems (Wanders et al., 2015) in the second order
557 statistics of the soil moisture retrievals; and (iv) SM retrieval products (and overpasses)
558 used in assimilation. Our improved results are based on soil moisture retrievals from
559 ascending overpasses only (versus both descending and ascending overpasses from
560 multiple datasets, i.e. AMSR-E/LSMEM, ASCAT and SMOS). Our exclusive focus on
561 the usefulness of soil moisture product promises more applicability especially for
562 improving satellite precipitation from the Global Precipitation Mission products. The
563 descending overpasses have generally better performance than the ascending, suggesting
564 the potentials of further improvements.

565 A quantitative comparison of Wanders et al. (2015) and our results is provided below.
566 Despite of the different time periods between Wanders et al. (2015, 2010-2011) and in
567 our study (2002-2007), Wanders et al. (2015) shows decreasing POD (-15.0% to -46.4%
568 depending on different products used) and FAR (-47.2% to -89.1% depending on
569 different products used) for all rainfall after assimilation using either (single or multiple)
570 SM products alone or SM + LST data combined (see Table 4 of Wanders et al., 2015).
571 While in our study, after applying Δ SM threshold, medium to large $3B42RT_{ADJ}$ rainfall
572 (≥ 2 mm/day) has an increase in POD (+6.6%) and decrease in FAR (-18.9%).
573 Furthermore, the significant dry bias in adjusted precipitation (see Fig.6 of Wanders et
574 al., 2015) is not present in our results (Figure 9). This is due to improvements in our
575 precipitation ensemble generation and bias correction scheme. Wanders et al. (2015)

577 applied an additional step generating precipitation particles sampling from a 3×3 window
578 that over-eliminates most of the excessive rainfall along with some real signal. We
579 suggest loosening this constraint to a larger window size or to sample from adjusted
580 precipitation instead of original 3B42RT precipitation. However sampling from adjusted
581 precipitation at each time step would significantly increase the computational demand,
582 limiting the potential for a global application at high temporal/spatial resolution.

583 Furthermore, the outcome is quite different for the distribution of soil moisture retrievals
584 after pre-processing (Fig.9 of Wanders et al. 2015 vs Figure 4 in our study) due to
585 different methods used. After pre-processing, distributions of soil moisture retrievals is
586 more similar to that of NLDAS precipitation forced, VIC modeled 1st layer soil moisture.
587 CDF-matching used by Wanders et al., (2015) is based on the assumption that satellite
588 soil moisture and modeled soil moisture respond to heavy rainfall in the same way –
589 essentially having a rank correlation of 1. However that is not observed because of
590 shallower detection depth of the satellite soil moisture. On the other hand, using the pre-
591 processing method presented in this study, the signal of near-saturation in AMSR-
592 E/LSMEM Δ SM tends to be overestimated after pre-processing, which indicates a heavy
593 rain event that is often accompanied with surface saturation and thus does not provide
594 effective information for the assimilation. The other benefit of the 2nd order polynomial
595 regression lies in its non-linearity. An error in the soil moisture product impacts the
596 precipitation adjustment in a predictable way, allowing for a more systematic post-
597 processing treatment. Based on the known error characteristics, we demonstrate a
598 potential remedy to deal with the error by applying a 2 mm/day cutoff Δ SM threshold.
599 Meanwhile, it is also highlighted that the cutoff threshold should be variable and
600 positively correlated with local soil moisture climatology. We acknowledge that the soil
601 moisture product used in Wanders et al. (2015), is a blended product of multiple satellite
602 soil moisture datasets. It is not clear how its error characteristics impact the adjusted
603 precipitation.

604 **6 Conclusion and Discussion**

605 Based on the retrieved soil moisture from AMSR-E using the LSMEM retrieval
606 algorithm, we propose an assimilation procedure to integrate soil moisture information

607 into the VIC land surface model so as to improve real-time, satellite precipitation
608 estimates. The ability to estimate rainfall amount is now enhanced with the above
609 improvements, especially for correcting medium rainfall amounts. However, constrained
610 by the noise in AMSR-E TBs and thus soil moisture retrievals, the assimilation is not
611 effective in detecting missed rainfall events. The improved precipitation estimates,
612 referred to as 3B42RT_{ADJ} estimates, are overall consistent in reproducing the spatial
613 pattern and time series of daily rainfall from NLDAS precipitation. The results illustrate
614 the potential benefits of using data assimilation to merge satellite retrievals of surface soil
615 moisture into a land surface model forced with real-time precipitation. Potentially the
616 method can be applied globally for areas meeting vegetation cover and surface condition
617 constraints that allows for soil moisture retrievals. Under these conditions, the approach
618 can provide a supplementary source of information for enhancing the quality of satellite
619 rainfall estimation, especially over poorly gauged areas like Africa.

620 Nonetheless, some caution is required. The results of this study show that the adjusted
621 real-time precipitation tends to add additional rain (frequency) resulting in more time
622 steps with rain but lower regional average in the western U.S. and slightly higher regional
623 average in the eastern U.S. It is also noticed that the precipitation adjustments are
624 insensitive under saturated soil moisture conditions. A wetter surface magnifies any error
625 associated with satellite observation by incorrectly adjusting precipitation. These errors,
626 mixed with the “real” signal, generally add approximately ~2mm of precipitation (or
627 higher) depending on the soil moisture climatology. It is important to consider these
628 circumstances when observations are used so as to avoid introducing additional error.
629 With these identified limitations, continued research is needed to assess the biases in the
630 real-time precipitation retrievals on a local to regional basis so the assimilation system
631 can be modified accordingly.

632 The assimilation scheme used here assumed that the errors were attributed to the real-
633 time precipitation retrievals, but the precipitation estimates after adjustment includes
634 errors from additional sources. The two primary sources are errors in soil moisture
635 retrievals and errors in the land surface model that include model parameterizations
636 (poorly or insufficiently represented processes as well as scale issues) and parameter
637 errors (insufficient calibration). There are also errors in other model forcing fields besides

638 precipitation. Further studies are needed to assess the attribution of these error sources to
639 the total error. Such research will further improve the use of real-time satellite-based
640 precipitation for global flood monitoring.

641 Besides the clear, heavy dependency of the assimilation effectiveness on the accuracy of
642 satellite soil moisture product, it is also important to acquire adequate knowledge on the
643 error characteristics of satellite soil moisture retrievals. Knowledge of the soil moisture
644 errors could be important and the assimilation methods (including precipitation ensemble
645 generation and pre-/post-processing method) should be chosen accordingly. On the other
646 hand, the presence of data gaps between overpasses could be a large source of uncertainty
647 with data assimilation. Further effort towards reliable spatial-temporal continuous (gap
648 filled) satellite soil moisture datasets is needed.

649 While it has been illustrated in this study that the enhancement of real time satellite
650 precipitation estimates can be realized through an assimilation approach using satellite
651 soil moisture data products and a particle filter, additional satellite-based observations
652 (e.g. multi-sensor soil moisture products) or variables (e.g. land surface temperatures as
653 shown in Wanders et al. 2015, inundated areas), could be added/replaced in the
654 assimilation process with different levels of complexity; e.g. by applying constraints on
655 the particle generation. This opens up a great number of opportunities in using space-
656 borne observations for supplementing direct retrievals of precipitation.

657 **Acknowledgements**

658 This research was supported through NASA grant NNX13AG97G (Multi-sensor
659 enhancement of real-time satellite precipitation retrievals for improved drought
660 monitoring) under the Precipitation Measurement Mission. Part of this research was
661 financially supported by NWO Rubicon 825.15.003. This support is gratefully
662 acknowledged.

663

664 **References**

- 665 Brocca, L., Melone, F., Moramarco, T. and Morbidelli, R.: Antecedent wetness
666 conditions based on ERS scatterometer data, *J. Hydrol.*, 364(1-2), 73–87,
667 doi:10.1016/j.jhydrol.2008.10.007, 2009.
- 668 Brocca, L., Moramarco, T., Melone, F. and Wagner, W.: A new method for rainfall
669 estimation through soil moisture observations, *Geophys. Res. Lett.*, 40(5), 853–858,
670 doi:10.1002/grl.50173, 2013.
- 671 Brocca, L., Ciabatta, L., Massari, C., Moramarco, T., Hahn, S., Hasenauer, S., Kidd, R.,
672 Dorigo, W., Wagner, W. and Levizzani, V.: Soil as a natural rain gauge: Estimating
673 global rainfall from satellite soil moisture data, *J. Geophys. Res. Atmos.*, 119(9), 5128–
674 5141, doi:10.1002/2014JD021489, 2014.
- 675 [Ciabatta, L., Brocca, L., Massari, C., Moramarco, T., Puca, S., Rinollo, A., Gabellani, S.,
676 and Wagner, W.: Integration of Satellite Soil Moisture and Rainfall Observations over the
677 Italian Territory, *J. Hydrometeorol.*, 16\(3\), 1341-1355, doi: 10.1175/JHM-D-14-0108.1,
678 2015.](#)
- 679 Chopin, F., Berges, J., Desbois, M., Jobard, I. and Lebel, T.: Satellite Rainfall Probability
680 and Estimation. Application to the West Africa During the 2004 Rainy Season, AGU
681 Spring Meet. Abstr., A12, 2005.
- 682 Crow, W. T.: Correcting land surface model predictions for the impact of temporally
683 sparse rainfall rate measurements using an ensemble Kalman filter and surface brightness
684 temperature observations, *J. Hydrometeorol.*, 4(5), 960–973, 2003.
- 685 Crow, W. T., Huffman, G. J., Bindlish, R. and Jackson, T. J.: Improving Satellite-Based
686 Rainfall Accumulation Estimates Using Spaceborne Surface Soil Moisture Retrievals, *J.*
687 *Hydrometeorol.*, 10(1), 199–212, doi:10.1175/2008JHM986.1, 2009.
- 688 Crow, W. T., Van Den Berg, M. J., Huffman, G. J. and Pellarin, T.: Correcting rainfall
689 using satellite-based surface soil moisture retrievals: The Soil Moisture Analysis Rainfall
690 Tool (SMART), *Water Resour. Res.*, 47(8), 1–15, doi:10.1029/2011WR010576, 2011.

691 Dee, D. P., Uppala, S. M., Simmons, A. J., Berrisford, P., Poli, P., Kobayashi, S., Andrae,
692 U., Balmaseda, M. A., Balsamo, G., Bauer, P. and others: The ERA-Interim reanalysis:
693 Configuration and performance of the data assimilation system, *Q. J. R. Meteorol. Soc.*,
694 137(656), 553–597, 2011.

695 Ebert, E. E., Janowiak, J. E. and Kidd, C.: Comparison of near-real-time precipitation
696 estimates from satellite observations and numerical models, *Bull. Am. Meteorol. Soc.*,
697 88(1), 47–64, doi:10.1175/BAMS-88-1-47, 2007.

698 Ek, M. B., Xia, Y., Wood, E., Sheffield, J., Luo, L., Lettenmaier, D., Livneh, B., Mocko,
699 D., Cosgrove, B., Meng, J., Wei, H., Koren, V., Schaake, J., Mo, K., Fan, Y. and Duan,
700 Q.: North American Land Data Assimilation System Phase 2 (NLDAS-2): Development
701 and Applications, *GEWEX Newsl.*, 21(2), 5–7, 2011.

702 Francois, C., Quesney, A. and Ottlé, C.: SAR Data into a Coupled Land Surface–
703 Hydrological Model Using an Extended Kalman Filter, *J. Hydrometeorol.*, 4(2), 473–487,
704 doi:10.1175/1525-7541(2003)4<473:SAOESD>2.0.CO;2, 2003.

705 Gao, H., Tang, Q., Shi, X., Zhu, C., Bohn, T. J., Su, F., She eld, J., Pan, M., and Wood,
706 E. F.: Water budget record from Variable Infiltration Capacity (VIC) model, in:
707 Algorithm Theoretical Basis Document for Terrestrial Water Cycle Data Records (in
708 review), 2010.

709 Huffman, G. J., Bolvin, D. T., Nelkin, E. J., Wolff, D. B., Adler, R. F., Gu, G., Hong, Y.,
710 Bowman, K. P. and Stocker, E. F.: The TRMM Multisatellite Precipitation Analysis
711 (TMPA): Quasi-Global, Multiyear, Combined-Sensor Precipitation Estimates at Fine
712 Scales, *J. Hydrometeorol.*, 8(1), 38–55, doi:10.1175/JHM560.1, 2007.

713 Huffman, G. J., Adler, R. F., Bolvin, D. T., and Nelkin, E. J.: The TRMM Multi-satellite
714 Precipitation Analysis (TMPA), in: *Satellite Rainfall Applications for Surface*
715 *Hydrology*, Springer Netherlands, 3–22, 2010.

716 Kalman, R. E.: A New Approach to Linear Filtering and Prediction Problems, *J. Basic*
717 *Eng.*, 82(1), 35, doi:10.1115/1.3662552, 1960.

718 Kerr, Y. H., Waldteufel, P., Richaume, P., Wigneron, J.-P., Ferrazzoli, P., Mahmoodi, A.,
719 Al Bitar, A., Cabot, F., Gruhier, C., Juglea, S. E., Leroux, D., Mialon, A. and Delwart, S.:

720 The SMOS Soil Moisture Retrieval Algorithm, *Geosci. Remote Sensing, IEEE Trans.*,
721 50(5), 1384–1403, doi:10.1109/TGRS.2012.2184548, 2012.

722 Liang, X., Lettenmaier, D. P., Wood, E. F. and Burges, S. J.: A simple hydrologically
723 based model of land surface water and energy fluxes for general circulation models, *J.*
724 *Geophys. Res.*, 99, 14415–14428, doi:10.1029/94JD00483, 1994.

725 Liang, X., Wood, E. F. and Lettenmaier, D. P.: Surface soil moisture parameterization of
726 the VIC-2L model: Evaluation and modification, *Glob. Planet. Change*, 13(1-4), 195–
727 206, doi:10.1016/0921-8181(95)00046-1, 1996.

728 Massari, C., Brocca, L., Moramarco, T., Trambly, Y. and Didon Lescot, J.-F.: Potential
729 of soil moisture observations in flood modelling: estimating initial conditions and
730 correcting rainfall, *Adv. Water Resour.*, 74, 44–53, doi:10.1016/j.advwatres.2014.08.004,
731 2014.

732 Matgen, P., Fenicia, F., Heitz, S., Plaza, D., de Keyser, R., Pauwels, V. R. N., Wagner,
733 W. and Savenije, H.: Can ASCAT-derived soil wetness indices reduce predictive
734 uncertainty in well-gauged areas? A comparison with in situ observed soil moisture in an
735 assimilation application, *Adv. Water Resour.*, 44, 49–65,
736 doi:10.1016/j.advwatres.2012.03.022, 2012.

737 McCabe, M. F., Wood, E. F. and Gao, H.: Initial soil moisture retrievals from AMSR-E:
738 Multiscale comparison using in situ data and rainfall patterns over Iowa, *Geophys. Res.*
739 *Let.*, 32(6), 1–4, doi:10.1029/2004GL021222, 2005.

740 Pan, M. and Wood, E. F.: Data Assimilation for Estimating the Terrestrial Water Budget
741 Using a Constrained Ensemble Kalman Filter, *J. Hydrometeorol.*, 7(3), 534–547,
742 doi:10.1175/JHM495.1, 2006.

743 Pan, M., Li, H. and Wood, E.: Assessing the skill of satellite-based precipitation
744 estimates in hydrologic applications, *Water Resour. Res.*, 46(9), W09535,
745 doi:10.1029/2009WR008290, 2010.

746 Pan, M., Sahoo, A. K. and Wood, E. F.: Improving soil moisture retrievals from a
747 physically-based radiative transfer model, *Remote Sens. Environ.*, 140, 130–140,
748 doi:10.1016/j.rse.2013.08.020, 2014.

749 Pellarin, T., Ali, A., Chopin, F., Jobard, I. and Bergès, J. C.: Using spaceborne surface
750 soil moisture to constrain satellite precipitation estimates over West Africa, *Geophys.*
751 *Res. Lett.*, 35(2), 3–7, doi:10.1029/2007GL032243, 2008.

752 Pellarin, T., Louvet, S., Gruhier, C., Quantin, G. and Legout, C.: A simple and effective
753 method for correcting soil moisture and precipitation estimates using AMSR-E
754 measurements, *Remote Sens. Environ.*, 136, 28–36, doi:10.1016/j.rse.2013.04.011, 2013.

755 Robock, A., Luo, L., Wood, E. F., Wen, F., Mitchell, K., Houser, P., Schaake, J.,
756 Lohmann, D., Cosgrove, B., Sheffield, J., Duan, Q., Higgins, W., Pinker, R., Tarpley, D.,
757 Basara, J. and Crawford, K.: Evaluation of the North American Land Data Assimilation
758 System over the southern Great Plains during the warm season, *J. Geophys. Res.*,
759 108(D22), 8846, doi:10.1029/2002JD003245, 2003.

760 Schaake, J. C., Duan, Q., Koren, V., Mitchell, K. E., Houser, P. R., Wood, E. F., Robock,
761 A., Lettenmaier, D. P., Lohmann, D., Cosgrove, B., Sheffield, J., Luo, L., Higgins, R. W.,
762 Pinker, R. T. and Tarpley, J. D.: An intercomparison of soil moisture fields in the North
763 American Land Data Assimilation System (NLDAS), *J. Geophys. Res. Atmos.*, 109(D1),
764 doi:10.1029/2002JD003309, 2004.

765 Schamm, K., M. Ziese, A. Becker, P. Finger, A. Meyer-Christoffer, U. Schneider, M.
766 Schröder, and P. Stender (2014), Global gridded precipitation over land: A description of
767 the new GPCP First Guess Daily product, *Earth Syst. Sci. Data*, 6, 49–60

768 Sorooshian, S.: Commentary-GEWEX (Global Energy and Water Cycle Experiment) at
769 the 2004 Joint Scientific Committee Meeting, *GEWEX Newsl.*, 14(2), 2, 2004.

770 Wanders, N., Pan, M. and Wood, E. F.: Correction of real-time satellite precipitation with
771 multi-sensor satellite observations of land surface variables, *Remote Sens. Environ.*, 160,
772 206–221, doi:10.1016/j.rse.2015.01.016, 2015.

773 Wu, H., Adler, R. F., Tian, Y., Huffman, G. J., Li, H. and Wang, J.: Real-time global
774 flood estimation using satellite-based precipitation and a coupled land surface and routing
775 model. *Water Resour. Res.*, 50(3), 2693-2717, doi:10.1002/2013WR014710, 2014.

776 **List of Tables**

777 **Tables**

778 Table 1 Error statistics of recovered precipitation and effect of surface saturation in the idealized experiment (mm/day).

779 Table 2 Error statistics of recovered NLDAS based on ΔSM (with added errors) conditioned on 1st layer soil wetness for the idealized
780 experiment (mm/day).

781 Table 3 Error statistics of 3B42RT and 3B42RT_{ADJ} compared to NLDAS precipitation (mm/day)

782 **List of Figures**

783 Figure 1 Schematic for the dynamic assimilation of AMSR-E/LSMEM Δ SM into TMPA
784 (3B42RT) with the particle filter (PF).

785 Figure 2 Schematic for the strategy for processing prior and posterior probability
786 densities in the particle filter.

787 Figure 3 Statistics of NLDAS precipitation given 3B42RT precipitation measurement.
788 Boxplot shows the minimum, 15% quantile, 30% quantile, median, 70% quantile, 85%
789 quantile and maximum value of NLDAS precipitation given 3B42RT precipitation in a
790 certain bin.

791 Figure 4 Empirical cumulative distribution function of changes in soil moisture from top
792 layer soil moisture from NLDAS precipitation forced VIC simulation (black), and
793 AMSR-E/LSMEM soil moisture retrieval before (red) and after (blue) pre-processing.

794 Figure 5 Two cases with recovered spatial rainfall pattern in the idealized experiment
795 after merging satellite soil moisture retrieval on: (a-e) 27th Oct. 2003 and (f-j) 22th Mar.
796 2006.

797 Figure 6 Accuracy of recovered precipitation in idealized experiment: (a) overall
798 performance and separately comparing the improvement performance of recovered
799 NLDAS precipitation (b) with and (c) without surface saturation condition. Statistics
800 provided in Table 1.

801 Figure 7 Error in recovered NLDAS precipitation given surface moisture condition.
802 Recovered NLDAS is based on using “truth” soil moisture and soil moisture with normal
803 error: $N(0,1\text{mm})$, $N(0,2\text{mm})$, $N(0,3\text{mm})$, $N(0,4\text{mm})$ and $N(0,5\text{mm})$. Statistics provided in
804 Table 2.

805 Figure 8 May 26th 2006 Rainfall pattern in 3B42RT (b) against NLDAS (d) as detected
806 by AMSR-E/LSMEM Δ SM (a), and recovered rainfall field ($3B42RT_{ADJ}$) by assimilating
807 AMSR-E/LSMEM Δ SM (c). Gray shading shows area without soil moisture retrievals.
808 Figure 9 Pearson correlation coefficient between AMSR-E/LSMEM Δ SM and
809 precipitation (from 2003/01/01 to 2007/07/31): a) NLDAS, b) 3B42RT and c)
810 $3B42RT_{ADJ}$; annual mean precipitation in d) NLDAS, e) 3B42RT and f) $3B42RT_{ADJ}$ of
811 time steps with AMSR-E/LSMEM Δ SM retrievals.
812 Figure 10 Frequency of rainy days in 3B42RT, $3B42RT_{ADJ}$ and NLDAS with a) 0.1
813 mm/day and b) 2 mm/day rainfall threshold to define a rain day.
814 Figure 11 Distribution of 3B42RT and $3B42RT_{ADJ}$ precipitation error compared to
815 NLDAS. Statistics are provided in Table 3.
816 Figure 12 FAR and POD of 3B42RT (top) and $3B42RT_{ADJ}$ (bottom) with a) 0.1 mm/day
817 and b) 2 mm/day rainfall threshold to define a rain event.
818 Figure 13 Probability that the added rainy days ($3B42RT = 0$ mm/day, $3B42RT_{ADJ} > 0$
819 mm/day) are true rain events (NLDAS > 0 mm/day) given corresponding AMSR-
820 E/LSMEM Δ SM.
821

Tables

Table 1 Error statistics of recovered precipitation and effect of surface saturation in the idealized experiment (mm/day).

		[3B42RT]- [Recovered NLDAS]-[NLDAS]	0	0~0.2	0.2~0.5	0.5~1.0	1.0~1.5	1.5~2	2~2.5	2.5~5.0	5.0~7.5	7.5~10	10~15	15~20	20~25	>25
All surface conditions	Bias		0.24	0.20	0.37	0.51	0.71	0.87	1.09	0.67	1.16	1.30	2.51	3.32	3.75	3.95
	MAE		0.40	0.42	0.66	0.86	1.14	1.41	1.70	1.48	2.24	2.63	4.21	5.56	6.70	9.76
Unsaturated surface	Bias		0.23	0.19	0.29	0.40	0.52	0.68	0.82	0.65	1.10	1.27	2.19	2.88	3.14	3.14
	MAE		0.39	0.41	0.59	0.75	0.95	1.21	1.43	1.45	2.17	2.58	3.88	5.11	6.07	8.94
Saturated surface	Bias		2.31	5.06	47.65	42.58	50.67	44.09	59.64	6.83	16.09	9.19	46.47	57.98	65.33	64.09
	MAE		3.35	5.54	48.71	43.73	52.43	46.96	61.85	9.64	21.42	15.01	49.07	60.78	69.53	70.73

Authors 10/2/2015 8:10 PM
Formatted Table

Table 2 Error statistics of recovered NLDAS based on ΔSM (with added errors) conditioned on 1st layer soil wetness for the idealized experiment (mm/day).

[VIC 1st layer SM] - [maximum]* [Recovered NLDAS]-[NLDAS] [mm/day]		<-30	-30~-25	-25~-20	-20~-15	-15~-12	-12~-10	-10~-9	-9~-8	>-8
No error	Median	0.04	0.03	0.02	0.02	0.02	0.03	0.03	0.04	0.16
	IQR	0.14	0.08	0.07	0.07	0.08	0.12	0.21	0.29	1.71
1.0	Median	0.86	1.07	1.08	1.03	0.99	0.97	0.97	0.94	0.66
	IQR	1.52	1.72	1.77	1.83	1.96	2.08	2.14	2.19	2.59
2.0	Median	0.68	1.07	1.40	1.56	1.52	1.44	1.51	1.64	1.54
	IQR	1.76	2.09	2.88	3.45	3.63	3.73	3.73	3.73	3.91
3.0	Median	0.15	0.80	1.20	1.41	1.47	1.51	1.65	1.84	1.88
	IQR	1.36	2.16	3.04	3.73	3.74	3.79	4.34	5.24	5.47
4.0	Median	0.22	0.56	0.83	1.15	1.30	1.40	1.63	1.88	1.97
	IQR	0.99	2.36	2.48	3.99	4.05	4.70	5.53	5.52	5.63
5.0	Median	0.00	0.15	0.52	0.90	1.10	1.27	1.54	1.81	1.89
	IQR	1.62	2.54	2.91	4.43	4.51	5.95	5.90	5.79	7.04

*1st layer soil depth is 100mm with a SM capacity of ~45mm depending on porosity.

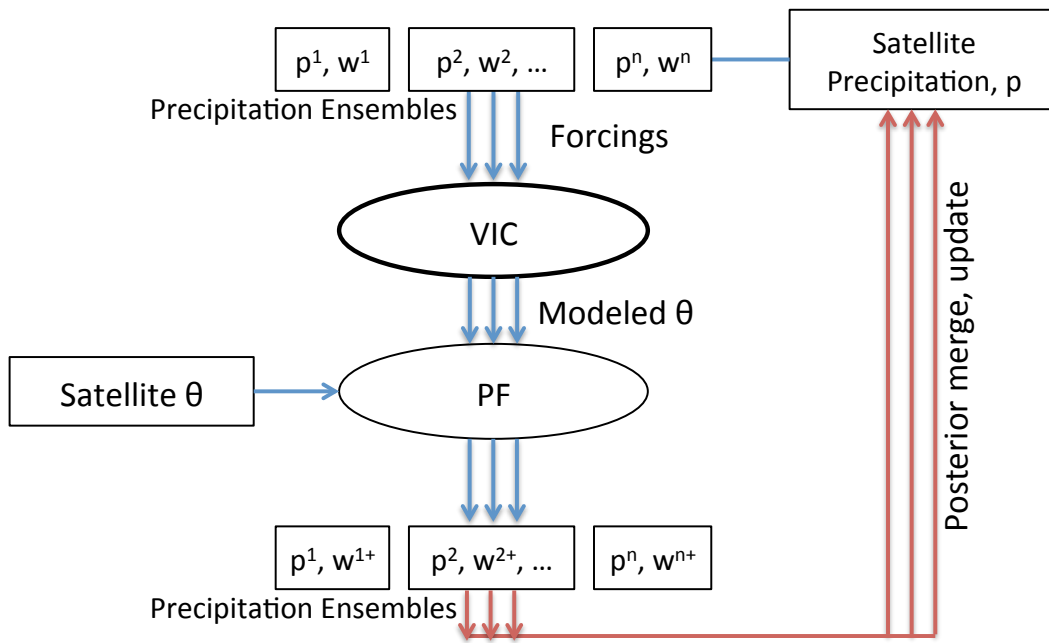
Authors 10/2/2015 8:10 PM
Formatted Table

Table 3 Error statistics of 3B42RT and 3B42RT_{ADJ} compared to NLDAS precipitation (mm/day)

[3B42RT] - [NLDAS] [mm/day]		<-25	-25~- 20	-20~- 15	-15~- 10	-10~- 5	-5~-2	-2~- 0.5	- 0.5~0 .5	0.5~2	2~5	5~10	10~1 5	15~2 0	20~2 5	>25
[3B42RT] - Mean		-32.32	-22.19	-17.13	-12.09	-6.98	-3.22	-1.09	-0.02	1.11	3.20	6.87	11.96	16.97	21.95	27.35
[NLDAS] STD		8.52	1.42	1.42	1.42	1.39	0.85	0.43	0.12	0.43	0.84	1.37	1.39	1.37	1.38	2.08
[3B42RT _{ADJ}]- Mean		-31.24	-20.31	-14.79	-9.69	-4.81	-1.60	0.16	1.08	0.44	0.21	0.02	-0.06	0.00	-0.03	-0.12
[NLDAS] STD		11.03	6.40	6.12	5.34	4.08	2.73	1.88	1.18	1.86	2.29	2.60	2.91	3.01	2.74	2.41

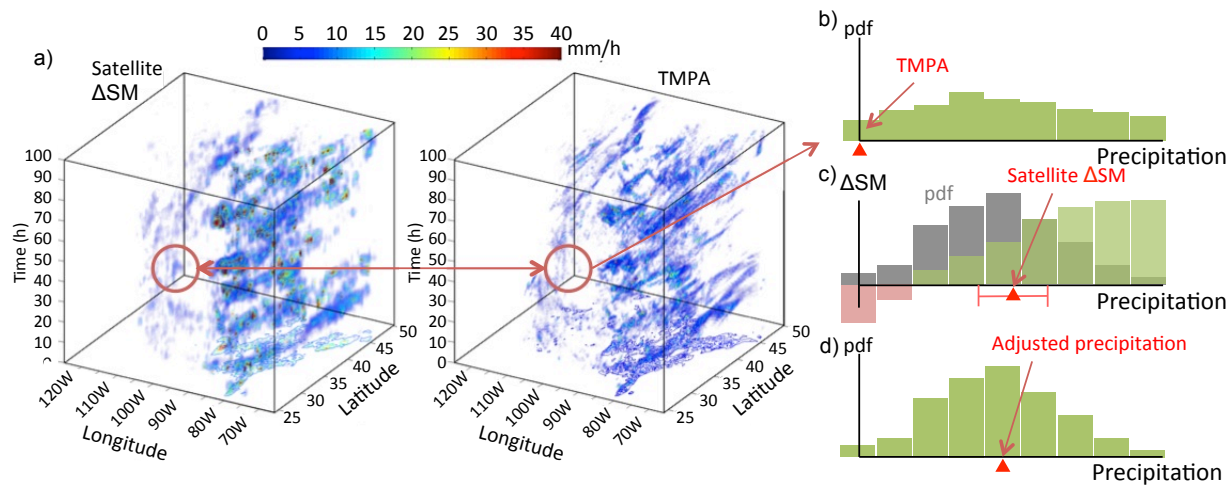
Authors 10/2/2015 8:10 PM
Formatted Table

829 **Figures**



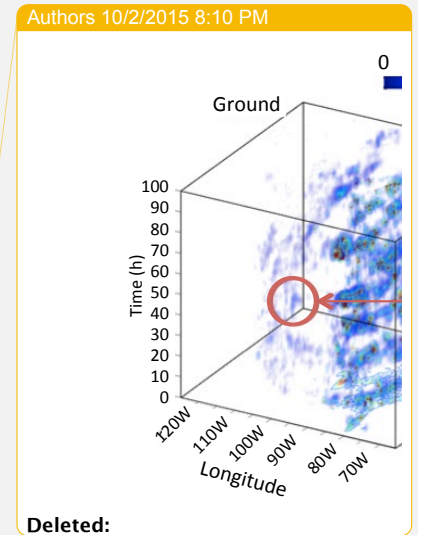
830

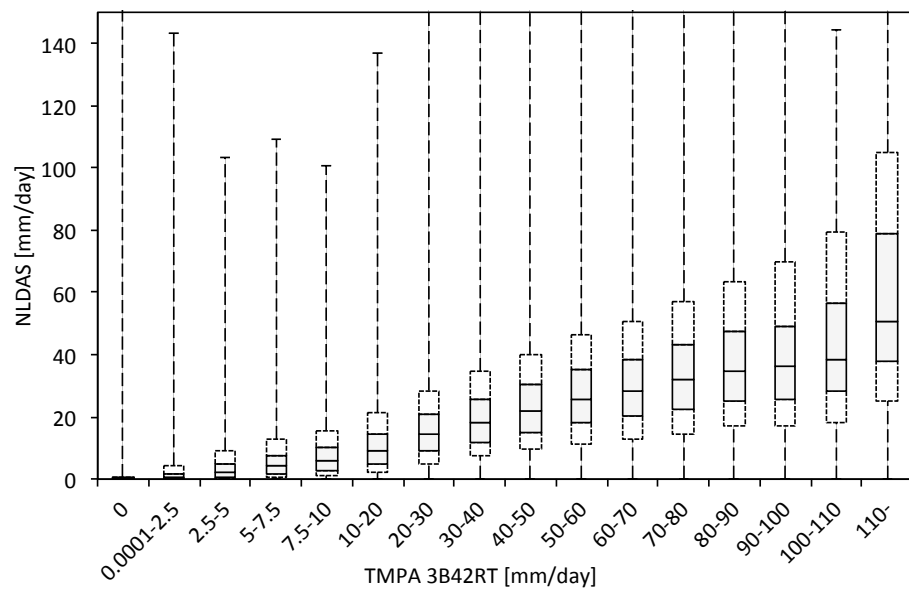
831 Figure 1 Schematic for the dynamic assimilation of AMSR-E/LSMEM Δ SM into TMPA (3B42RT) with the particle filter (PF).



832

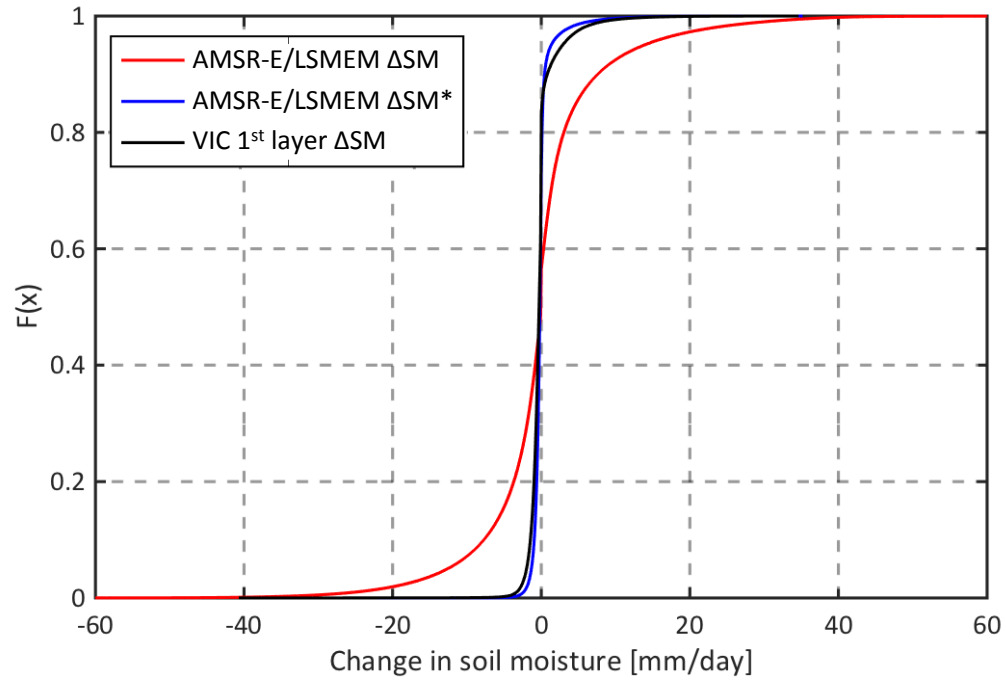
833 Figure 2 Schematic for the strategy for processing prior and posterior probability densities in the particle filter. The missing rainfall
 834 event in TMPA (circled in the right panel of a), correspond to red triangle in b)) against satellite signals as detected by AMSR-
 835 E/LSMEM Δ SM (circled in the left panel of a), correspond to red triangle in c)), and recovered by assimilating AMSR-E/LSMEM
 836 Δ SM into TMPA (marked by red triangle in d)).





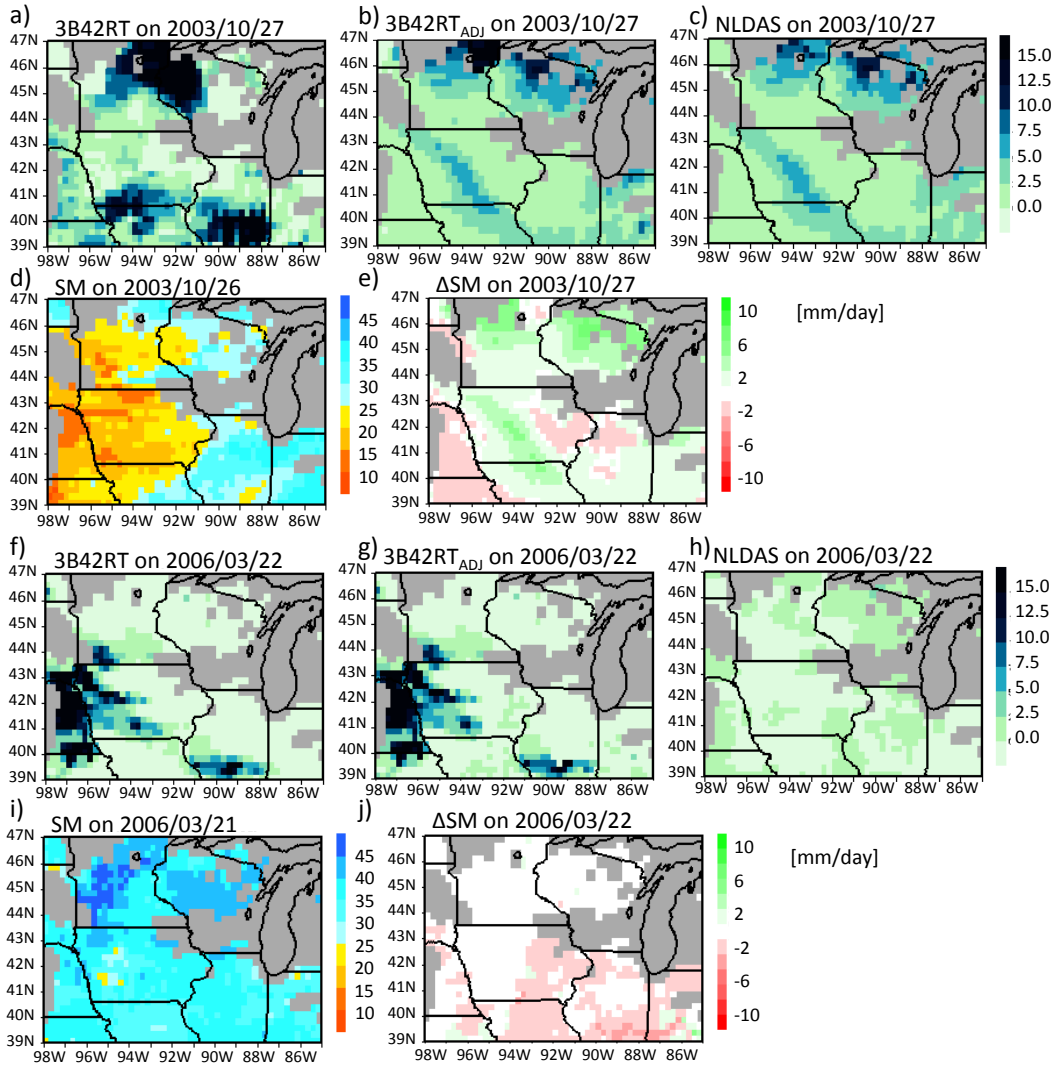
838

839 Figure 3 Statistics of NLDAS precipitation given 3B42RT precipitation measurement. Boxplot shows the minimum, 15% quantile,
 840 30% quantile, median, 70% quantile, 85% quantile and maximum value of NLDAS precipitation given 3B42RT precipitation in a
 841 certain bin.



842

843 Figure 4 Empirical cumulative distribution function of changes in soil moisture from top layer soil moisture from NLDAS
 844 precipitation forced VIC simulation (black), and AMSR-E/LSMEM soil moisture retrieval before (red) and after (blue) pre-
 845 processing.



346

347 Figure 5 Two cases with recovered spatial rainfall pattern in the idealized experiment after merging satellite
 348 soil moisture retrieval on: (a-e) 27th Oct. 2003 and (f-j) 22th Mar. 2006.

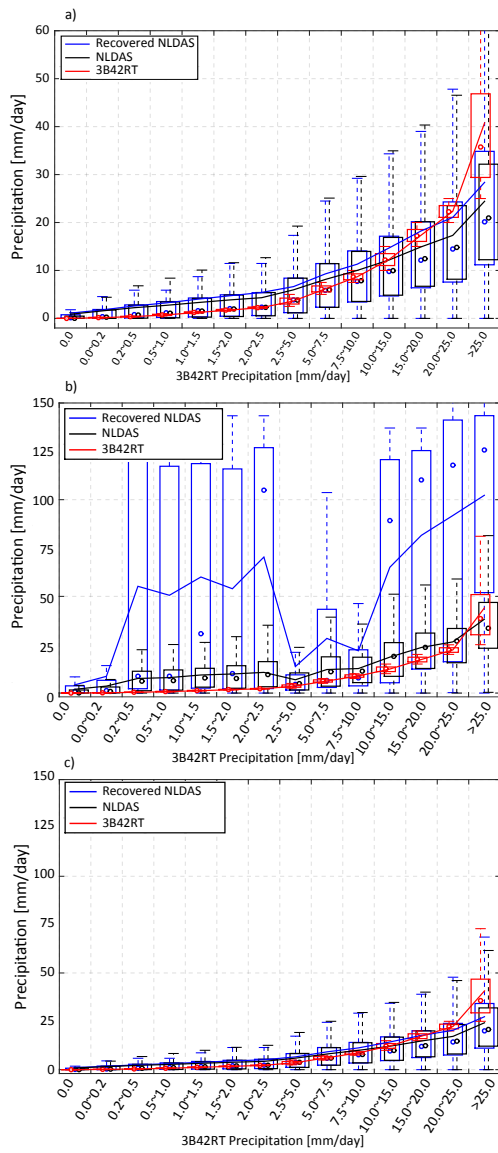
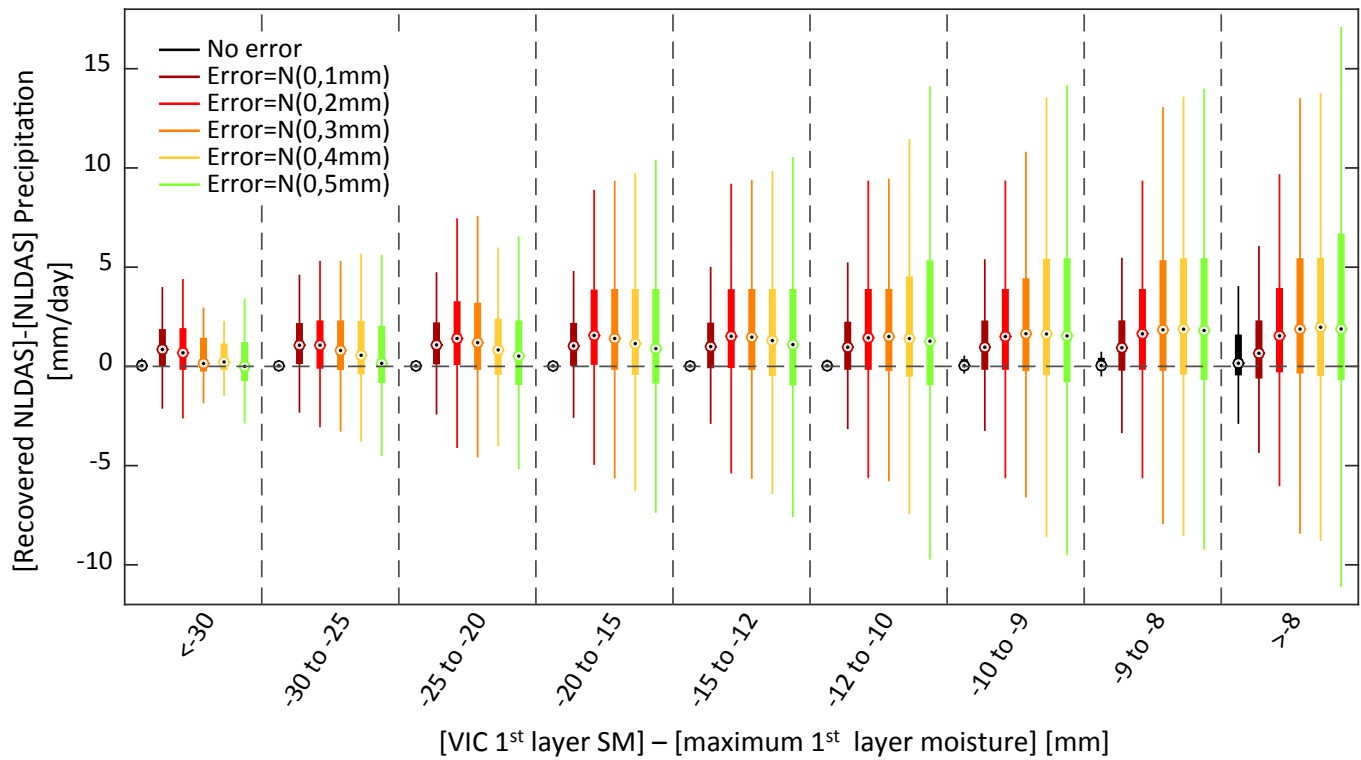
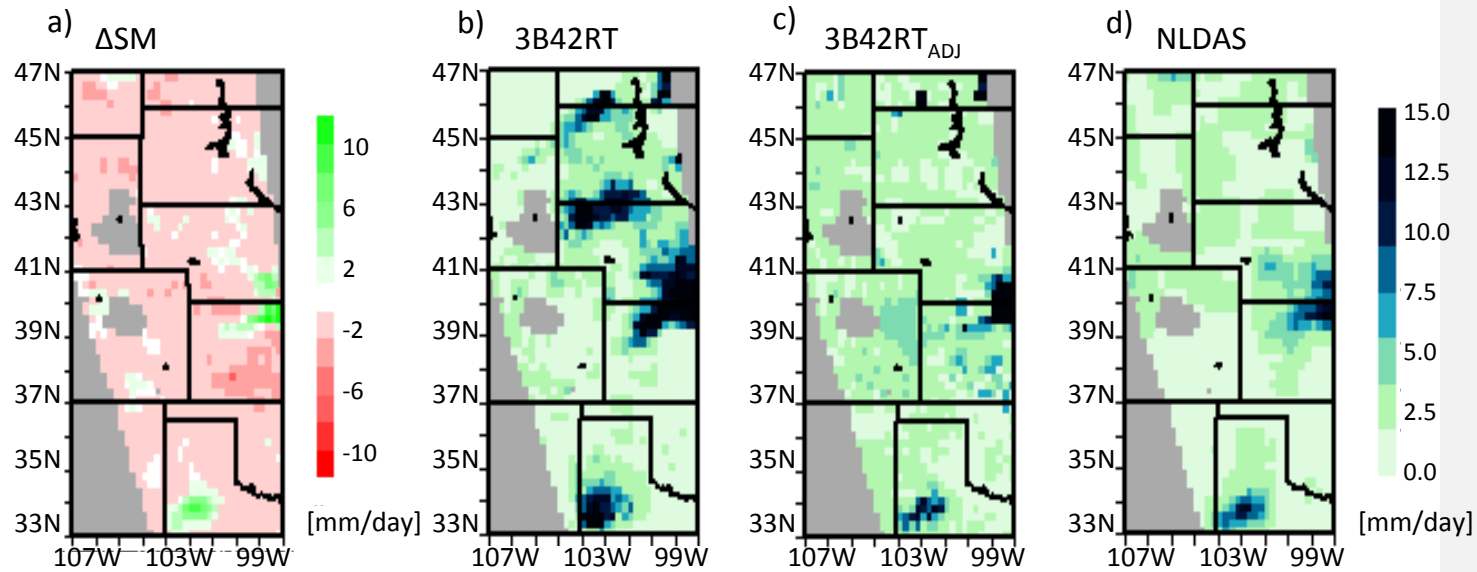


Figure 6 Accuracy of recovered precipitation in idealized experiment: (a) overall performance and separately comparing the improvement performance of recovered NLDAS precipitation (b) with and (c) without surface saturation condition. Statistics provided in Table 1.



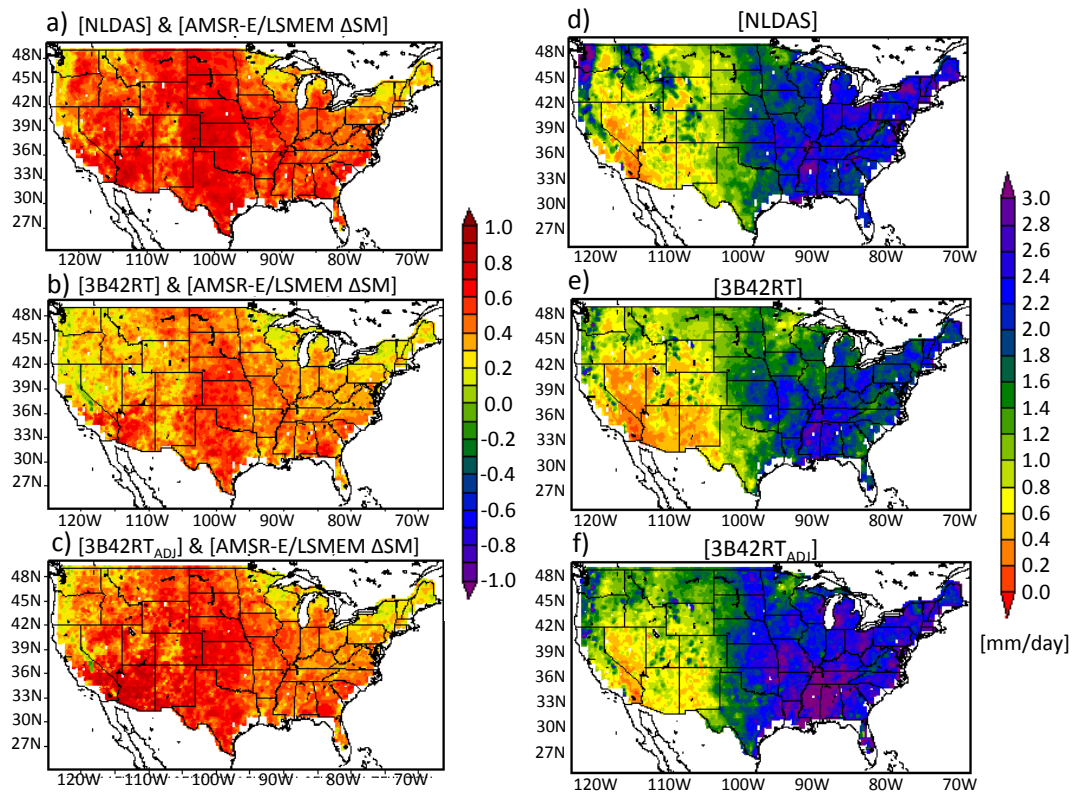
850

851 Figure 7 Error in recovered NLDAS precipitation given surface moisture condition. Recovered NLDAS is based on using “truth” soil
 852 moisture and soil moisture with normal error: $N(0,1\text{mm})$, $N(0,2\text{mm})$, $N(0,3\text{mm})$, $N(0,4\text{mm})$ and $N(0,5\text{mm})$. Statistics provided in
 853 Table 2.



854

855 Figure 8 May 26th 2006 Rainfall pattern in 3B42RT (b) against NLDAS (d) as detected by AMSR-E/LSMEM ΔSM (a), and recovered
 856 rainfall field (3B42RT_{ADJ}) by assimilating AMSR-E/LSMEM ΔSM (c). Gray shading shows area without soil moisture retrievals.

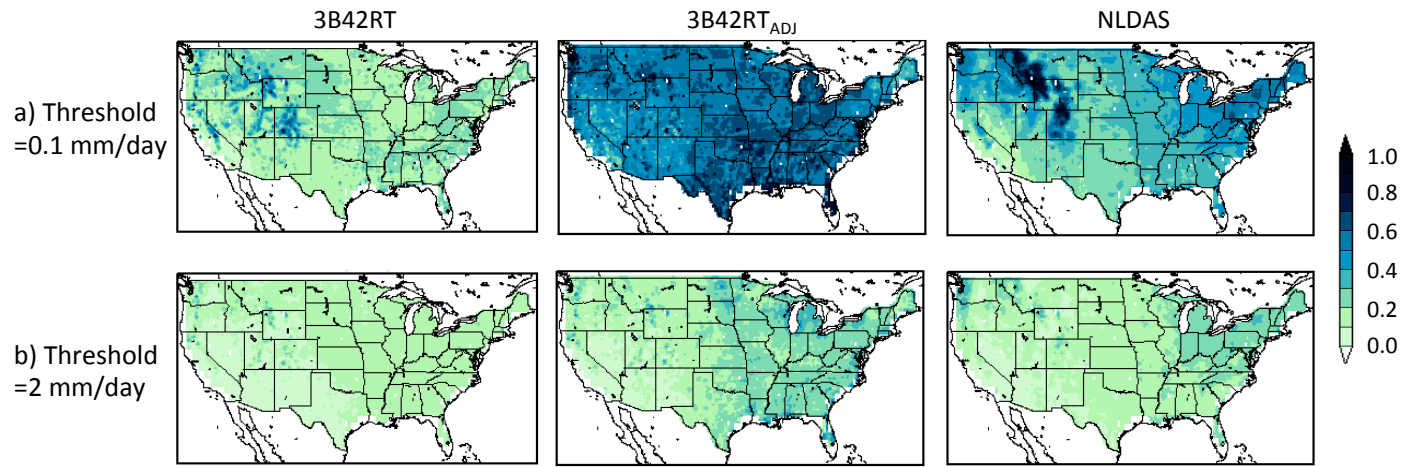


857

858 | Figure 9 Pearson correlation coefficient between AMSR-E/LSMEM Δ SM and precipitation (from 2003/01/01 to 2007/07/31): a)
 859 NLDAS, b) 3B42RT and c) 3B42RT_{ADJ}; annual mean precipitation in d) NLDAS, e) 3B42RT and f) 3B42RT_{ADJ} of time steps with
 860 AMSR-E/LSMEM Δ SM retrievals.

Authors 10/2/2015 8:10 PM

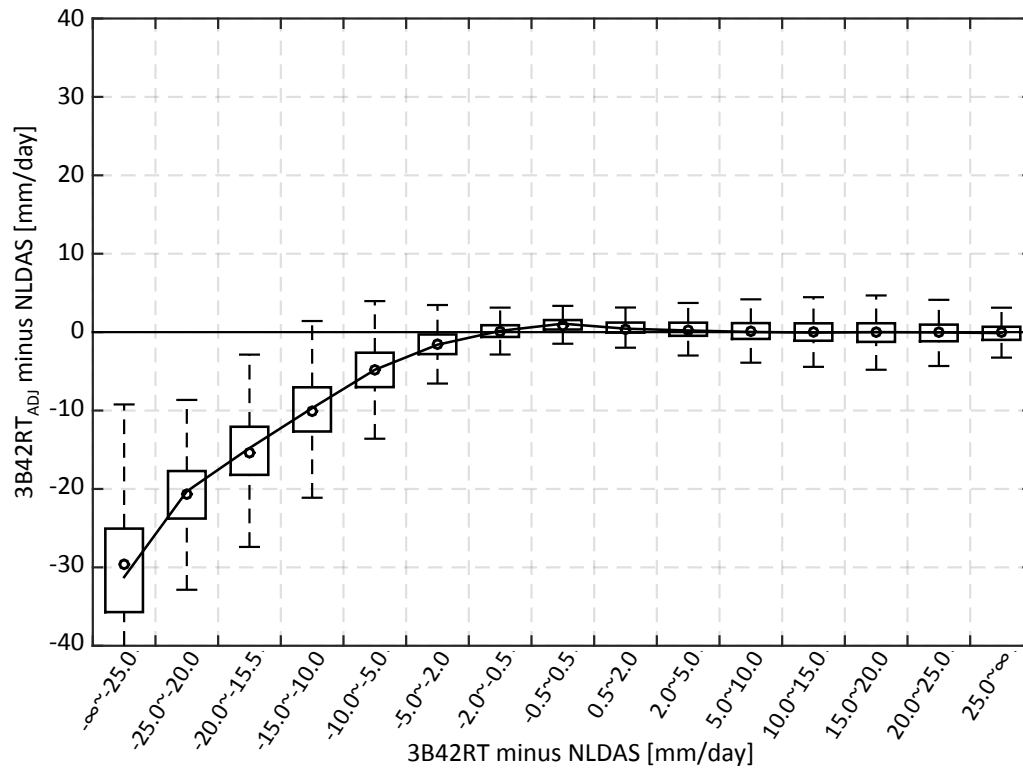
Deleted: :



862

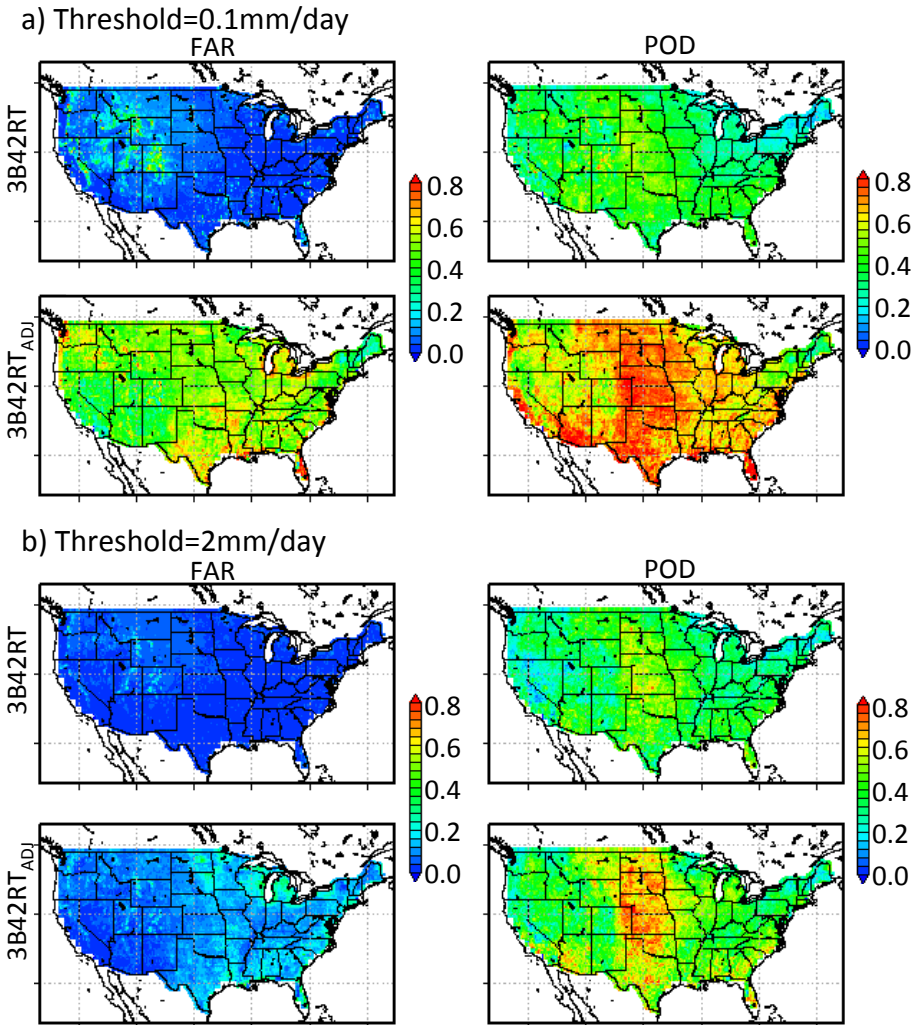
863 Figure 10 Frequency of rainy days in 3B42RT, 3B42RT_{ADJ} and NLDAS with a) 0.1 mm/day and b) 2 mm/day rainfall threshold to

864 define a rain day.



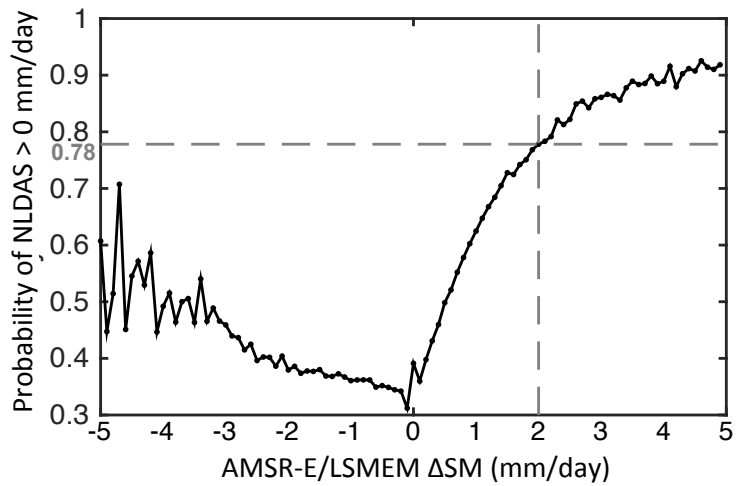
865

866 Figure 11 Distribution of 3B42RT and 3B42RT_{ADJ} precipitation error compared to NLDAS. Statistics are provided in Table 3.



867

868 Figure 12 FAR and POD of 3B42RT (top) and 3B42RT_{ADJ} (bottom) with a) 0.1 mm/day and b) 2
 869 mm/day rainfall threshold to define a rain event. The significant increase in FAR for all rainfall events
 870 (bottom left, a) is not present for rainfall larger than 2 mm/day (bottom left, b)).



871

872 Figure 13 Probability that the added rainy days ($3B42RT = 0$ mm/day, $3B42RT_{ADJ} > 0$ mm/day) are
 873 true rain events (NLDAS > 0 mm/day) given corresponding AMSR-E/LSMEM Δ SM.

874